

Model uncertainty estimation in data assimilation for multi-scale systems with partially observed resolved variables

S. Pathiraja¹, P.J. Van Leeuwen²

¹*Institut für Mathematik, Universität Potsdam, Germany*

²*Department of Meteorology and National Centre for Earth Observation, University of Reading, United Kingdom*

Abstract

Model uncertainty quantification is an essential component of effective Data Assimilation (DA), although it can be a challenging task for complex partially observed non-linear systems with highly non-Gaussian uncertainties. Model errors associated with sub-grid scale processes are of particular interest in meteorological DA studies; these are often represented through stochastic parameterizations of the unresolved process. Many existing Stochastic Parameterization schemes are only applicable when knowledge of the true sub-grid scale process or full observations of the coarse scale process are available, which is typically not the case in real applications. We present a methodology for estimating the statistics of sub-grid scale processes for the more realistic case that only partial observations of the coarse scale process are available. The aim is to first estimate the conditional probability density of additive model errors given the state of the system, from which samples can be generated to simulate model error within any ensemble-based assimilation framework. Model error realizations are estimated over a training period by

minimizing their conditional variance, constrained by available observations. Special is that these errors are binned conditioned on the previous model state during the minimization process, allowing for the recovery of complex non-Gaussian error structures. We demonstrate the efficacy of the approach through numerical experiments with the multi-scale Lorenz 96 system. Various parameterizations of the Lorenz 96' model are considered with both small and large time scale separations between slow (coarse scale) and fast (fine scale) variables. Results indicate that both error estimates and forecasts are improved with the proposed method compared to two existing methods for accounting for model uncertainty in DA.

Keywords: Data Assimilation, Model Error, Multi-Scale, Non-Gaussian, Uncertainty Quantification

1. Introduction

Model Uncertainty quantification is one of the central challenges in successfully utilizing any Data Assimilation method; the optimal combination of forecasts and measurements is critically dependent on the uncertainties assigned to each. Model errors can arise from a range of sources, including but not limited to: model discretization errors in space and time, unresolved sub-grid processes, and uncertainties in model forcing or input data. The lack of complete high resolution and high quality verification data makes model error estimation difficult in most real world applications. There is an increasing recognition of the need to develop methods capable of accurately quantifying model error, particularly in relation to errors arising from unre-

solved spatial and temporal scales.

Early methods for characterizing model error in ensemble data assimilation involved using inflation and localization techniques which aim to modify the sample covariance [e.g. Anderson and Anderson, 1999; Hamill et al., 2001; Houtekamer and Mitchell, 2001]. These were initially developed as a heuristic remedy for filter divergence in Ensemble Kalman filtering and to reduce the effects of sampling errors in the sample covariance matrix due to the use of small ensemble sizes. The increase in forecast variance (or trace of the covariance matrix) associated with inflation methods also has the added benefit of at least partially accounting for forecast model errors. In additive inflation [Anderson and Anderson, 1999] the of the forecast covariance matrix is increased by some additive term $\lambda > 0$ whilst in multiplicative inflation [Anderson, 2001], all elements of the covariance matrix are multiplied by an λ typically > 1 . However, the inflation parameter λ must be numerically tuned (although there have been recent advances in estimating inflation parameters more objectively [Anderson, 2007; Miyoshi, 2011; Liang et al., 2012]). A more explicit treatment of model error involves estimating a forecast bias term, which can be considered as stochastic or deterministic. This can be estimated from the difference in mean analyses and forecasts [e.g. Saha, 1992; Dee, 1995], using the difference between 2 forecast models of differing resolution [Hamill and Whitaker, 2005] or online within the data assimilation system by incorporating a constant additive term to be updated alongside the system states [e.g. Dee and Da Silva, 1998]. However, these methods are limited in that the focus is only on the first moment. More

complex methods involve estimating a parameterization on-line using prior knowledge to define the potentially non-linear functional form of model errors [e.g. Lang et al., 2016].

In the Variational Data Assimilation literature, model error is often considered by formulating the forecast model as a weak constraint in the optimization problem (often referred to as Weak constraint 4D-VAR) [Zupanski, 1997; Tremolet, 2006]. One approach to achieve this is through Long-window 4D-VAR, where an additive model error term is incorporated as a control variable in the 4D-Var formulation, with initial conditions for each window held fixed [Fisher et al., 2005; Tremolet, 2006; Fisher et al., 2011]. These approaches require a priori specification of the model error covariance matrix, which can be a challenging task. More recently, there has been renewed interest in off-line estimation of model error statistics using analysis increments (i.e. difference between forecast and analysis) from a data assimilation run [Rodwell and Palmer, 2007; Mitchell and Carrassi, 2015]. Both the on-line and off-line error estimation methods suffer from the common drawback that the error estimates are affected by deficiencies in the assimilation algorithm itself.

There has been a recent flurry of research activity in using stochastic parameterization and model reduction methods to account for model errors associated with unresolved sub-grid scale processes in data assimilation [Mitchell and Gottwald, 2012; Berry and Harlim, 2014; Mitchell and Carrassi, 2015; Lu et al., 2017, e.g]. This is particularly relevant in weather and climate

modelling where the system dynamics evolve on a wide range of spatial and temporal scales. Such model reduction methods involve modelling or parameterizing sub-grid scale processes in a more computationally tractable fashion than solving the true sub-grid differential equations. Often this is achieved through either deterministic or stochastic parameterizations which aim to capture the mean effects of small scale processes on the resolved variables. Several studies have demonstrated the superiority of stochastic over purely deterministic parameterizations in this regard [Buizza et al., 1999; Palmer, 2001]. Methods for stochastic parameterizations of multi-scale systems vary widely; from homogenization methods that are suited to systems with large time scale separations [Pavliotis and Stuart, 2008; Wouters et al., 2016] to fitting stochastic models to sub-grid tendencies [Wilks, 2005; Arnold et al., 2013, e.g]. Methods of the form of the latter include that of Crommelin and Vanden-Eijnden [2008], who proposed utilising a Conditional Markov Chain to represent the evolution of sub-grid tendencies given the state of the resolved variable. Kwasniok [2012] explored a similar approach whereby a clustering algorithm was used to develop a cluster-weighted Markov chain to represent the sub-grid tendencies. Arnold et al. [2013] extended the work of Wilks [2005] by examining the potential of autoregressive error models to effectively parameterize sub-grid tendencies in the multi-scale Lorenz 96 system. More recently, Lu et al. [2017] have proposed using a non-Markovian non-linear autoregressive moving average model to characterize model error. All of the aforementioned approaches require knowledge of the sub-grid scale equations, representative data of the sub-grid tendencies and/or full observations of the resolved variables. This reduces their applicability for more

realistic Data Assimilation applications where knowledge of the sub-grid scale processes is unavailable and the resolved variables are only partially observed.

This work aims to propose a methodology for model uncertainty estimation in such a setting. It is specifically designed for partially observed systems and requires no a priori knowledge of the sub-grid scale processes. The method is suited to systems where a locality and symmetry assumption can be invoked, as this is used to regularize the ill-posed problem of estimating model errors from partial observations. In such systems, errors due to sub-grid scale processes are dependent only on neighboring states instead of the full resolved state vector, and the error statistics are the same at each location in space, or over larger parts of state space with similar physics. The approach aims to first estimate the conditional probability density of additive model errors given the state of the system. Additive errors are estimated at a time resolution equal to the observation interval. Samples from this density can then be combined with forward model simulations to generate a forecast density in any ensemble-based data assimilation framework. Model errors are estimated over a training period by minimizing their conditional variance, constrained by available observations. Special is that these errors are binned conditioned on the previous model state during the minimization process, allowing for the recovery of complex error structures. Finally, the use of nonparametric density estimation techniques allows for the characterization of highly non-Gaussian errors. We demonstrate its efficacy through numerical experiments with the multi-scale Lorenz 96 system. The forecast model in the assimilation experiment is the single layer Lorenz 96, so that

model errors arise from the unresolved high frequency fast variables. The proposed approach is compared to two benchmark methods in terms of the ability to recover the true model error structure and the impact on assimilation and forecast quality.

The remainder of this paper is structured as follows. In Section 2, we discuss Data Assimilation methods and the Ensemble Transform Kalman Filter (ETKF), which is adopted as the assimilation algorithm in this study. Methods for accounting for model uncertainty in Data Assimilation for partially observed systems are discussed in Section 3. The details of the proposed method are provided, along with a long window 4D-VAR formulation and ensemble analysis increment based method, both of which are adopted as benchmarks. In Section 4 we describe the numerical experiments with the multi-scale Lorenz 96' system. We conclude with a summary of the main outcomes and possibilities for future work in Section 5.

2. Data Assimilation Methods

The general problem setting considered in this study is described as follows. Suppose the system of interest can be represented by the following discrete time continuous state space equation:

$$\mathbf{x}_j = M(\mathbf{x}_{j-1}) + \boldsymbol{\eta}_j \tag{1}$$

where $\mathbf{x}_{j-1} \in \mathbb{R}^{N_x}$ is the true state vector at time $j - 1$; $M : \mathbb{R}^{N_x} \rightarrow \mathbb{R}^{N_x}$ is a Markov Order 1 forecast model; and $\boldsymbol{\eta}_j \in \mathbb{R}^{N_x}$ is an additive model error

at time j capturing deficiencies in the forecast model M .

Suppose also that noisy partial observations of the state \mathbf{x}_j are available, given by the following:

$$\mathbf{y}_j = \mathbf{H}\mathbf{x}_j + \boldsymbol{\varepsilon}_j \quad (2)$$

where $\mathbf{H} : \mathbb{R}^{N_x} \rightarrow \mathbb{R}^{N_y}$ is a $N_y \times N_x$ matrix consisting of 1's and 0's only; $\mathbf{y}_j \in \mathbb{R}^{N_y}$ is the vector of observations at time j ; and $\boldsymbol{\varepsilon}_j \in \mathbb{R}^{N_y}$ is the observation noise at time j , assumed to be temporally uncorrelated Gaussian with zero mean and known covariance matrix $\mathbf{R} \in \mathbb{R}^{N_y \times N_y}$. In this study, we focus on the case $N_y < N_x$, i.e. the state vector is partially observed, so that the sum of each row of \mathbf{H} is 1. Additionally, we consider the case where observations are available at a coarser temporal resolution than the model forecast time step. Throughout the manuscript, the notation $\mathbf{x}[k]$ is used to refer to the k th element of the vector \mathbf{x} ; $\mathbf{X}[k, l]$ refers to the element at the k th row and l th column of the matrix \mathbf{X} .

The aim of data assimilation is to optimally combine observations and prior information (usually from a numerical model, e.g. equation 1) based on their respective uncertainties. The standard discrete time Kalman filter provides the optimal posterior (in the minimum variance sense) for the special case of linear forecast model and observation operator, and for zero mean temporally uncorrelated Gaussian process and observation noise. Ensemble Kalman Filter methods (amongst others) have been developed to improve their applicability for the more general case of non-linear and non-Gaussian problems encountered in many applications. The Ensemble Trans-

form Kalman Filter (ETKF) [Bishop et al., 2001; Wang et al., 2004] has been widely adopted particularly in meteorological Data Assimilation due to its computational efficiency and accuracy in high dimensional systems with small ensemble sizes when localization is applied. The ETKF is discussed in the remainder of this section.

2.1. Ensemble Transform Kalman Filter

The ETKF is an extension of the original Ensemble Kalman Filter (EnKF) proposed by Evensen [1994]. It belongs to the class of Ensemble Square Root Filters; these methods operate on the square root of the forecast and analysis error covariance rather than the full covariance matrices [Tippett et al., 2003]. Such methods involve developing a deterministic transformation that maps the forecast ensemble to the analysis ensemble whose statistics are consistent with the Kalman Filter update. This is particularly important whenever the ensemble size $n \ll$ dimension of the state N_x , as the sample covariance matrix will be rank deficient thereby underestimating the true error covariance. As noted by Tippett et al. [2003], the linear transformation is not uniquely defined, and is the main distinguishing factor between different ensemble square root methods. Here we present the method of Wang et al. [2004], which is an updated version of the original ETKF proposed by Bishop et al. [2001] that ensures the filter is unbiased. A single cycle of the ETKF proceeds as follows:

A forecast ensemble at time j (denoted \mathbf{X}_j^f) is generated by propagating

the analysis ensemble from the previous time through equation 3:

$$\mathbf{x}_j^{fi} = M(\mathbf{x}_{j-1}^{ai}) + \boldsymbol{\eta}_j^i \quad \forall \quad i \in \{1, \dots, n\} \quad (3)$$

$$\mathbf{X}_j^f = \left[\mathbf{x}_j^{f1}, \dots, \mathbf{x}_j^{fn} \right] \in \mathbb{R}^{N_x \times n} \quad (4)$$

where the superscripts f and a denote the forecast and analysis, respectively. For the purposes of calculating the square root update, further computations are carried out using the forecast ensemble deviation matrix $\mathbf{X}_j^{f'}$:

$$\mathbf{X}_j^{f'} = \mathbf{X}_j^f - \bar{\mathbf{x}}_j^f \mathbf{k} \in \mathbb{R}^{N_x \times n} \quad (5)$$

where:

$$\mathbf{k} = \left[1, \dots, 1 \right] \in \mathbb{R}^n$$

$$\bar{\mathbf{x}}_j^f = \frac{1}{n} \sum_{i=1}^n \mathbf{x}_j^{fi}$$

The standard Kalman Filter analysis equations for the mean state $\bar{\mathbf{x}}_j^a$ and covariance \mathbf{P}_j^a are given by:

$$\bar{\mathbf{x}}_j^a = \bar{\mathbf{x}}_j^f + \mathbf{K}_j(\mathbf{y}_j - \mathbf{H}\bar{\mathbf{x}}_j^f) \quad (6)$$

$$\mathbf{P}_j^a = (\mathbf{I} - \mathbf{K}_j\mathbf{H})\mathbf{P}_j^f \quad (7)$$

$$\mathbf{K}_j = \mathbf{P}_j^f \mathbf{H}^T (\mathbf{H}\mathbf{P}_j^f \mathbf{H}^T + \mathbf{R})^{-1} \quad (8)$$

where $\mathbf{I} \in \mathbb{R}^{N_x \times N_x}$ is the identity matrix, and the superscript T refers to the transpose operator.

The crucial strength of ensemble Kalman filters in general is that one can avoid the explicit calculation of the state covariance matrices. In the ETKF, this is achieved by writing the analysis ensemble deviation matrix in terms of the forecast ensemble deviation matrix as:

$$\mathbf{X}_j^{a'} = \mathbf{X}_j^{f'} \mathbf{T} \quad (9)$$

where $\mathbf{T} \in \mathbb{R}^{n \times n}$ is computed using a Singular Value Decomposition (SVD) of the scaled forecast ensemble observation deviation matrix. This approach transforms the computations to ensemble space which significantly reduces the required number of operations whenever $n \ll N_y$ (as is typically the case in real world geophysical applications). The transformation matrix \mathbf{T} can be found as follows. Using the definition of the empirical covariance matrix $\mathbf{P}_j = \frac{1}{n-1} \mathbf{X}_j [\mathbf{X}_j]^T$ in equation 7, together with the Sherman-Morrison-Woodbury identity, one can obtain

$$\mathbf{X}_j^{a'} [\mathbf{X}_j^{a'}]^T = \mathbf{X}_j^{f'} \left(\mathbf{I} + \frac{1}{n-1} [\mathbf{H}\mathbf{X}_j^{f'}]^T \mathbf{R}^{-1} \mathbf{H}\mathbf{X}_j^{f'} \right) [\mathbf{X}_j^{f'}]^T \quad (10)$$

Equation 9 implies that

$$\mathbf{T}\mathbf{T}^T = \left(\mathbf{I} + \frac{1}{n-1} [\mathbf{H}\mathbf{X}_j^{f'}]^T \mathbf{R}^{-1} \mathbf{H}\mathbf{X}_j^{f'} \right)^{-1} \quad (11)$$

$$= (\mathbf{I} + \mathbf{W}^T \mathbf{W})^{-1} \quad (12)$$

Using the SVD of

$$\mathbf{W} = \frac{1}{\sqrt{n-1}} \left([\mathbf{X}_j^{f'}]^T \mathbf{H}^T \mathbf{R}^{-1/2} \right) = \mathbf{U}\mathbf{\Sigma}\mathbf{V}^T \quad (13)$$

we can identify

$$\mathbf{T} = \mathbf{U}(\mathbf{I} + \Sigma \Sigma^T)^{-1/2} \mathbf{U}^T \quad (14)$$

Furthermore, the SVD of \mathbf{W} is utilized to efficiently calculate the analysis ensemble mean $\bar{\mathbf{x}}_j^a$:

$$\bar{\mathbf{x}}_j^a = \bar{\mathbf{x}}_j^f + \frac{1}{\sqrt{n-1}} \mathbf{X}_j^{f'} \mathbf{U} (\Sigma^T \Sigma + \mathbf{I})^{-1} \Sigma \mathbf{V}^T \mathbf{R}^{-1/2} (\mathbf{y}_j - \mathbf{H} \bar{\mathbf{x}}_j^f) \quad (15)$$

Finally, the analysis ensemble is determined by adding the analysis deviation matrix $\mathbf{X}_j^{a'}$ to the analysis ensemble mean: $\bar{\mathbf{x}}_j^a$:

$$\mathbf{X}_j^a = \bar{\mathbf{x}}_j^a \mathbf{k} + \mathbf{X}_j^{a'} \quad (16)$$

3. Accounting for Model Uncertainty

Data assimilation outputs are critically dependent on the uncertainty assigned to both model simulations and observations. Furthermore, Kalman filter methods do not directly account for model or observation bias, meaning that systematic errors must be accounted for externally. In the following, we propose a method for estimating model uncertainty in partially observed systems where knowledge of the unresolved processes is unavailable. The approach is specifically for use with Monte-Carlo based sequential filtering techniques such as Ensemble Kalman methods and Particle methods. Existing methods for accounting for model errors that are amenable to the partially observed setting are also discussed in Section 3.2.

3.1. Proposed Method

The proposed method utilizes a training period in order to gather estimates of the additive errors for the entire state vector (both observed and unobserved). Estimates are generated using an optimization procedure that aims to minimize the conditional variance of the model errors given the state at the previous time, constrained by the available observations. This approach allows for the estimation of complex state dependent error structures without prior knowledge of their functional form. This is particularly relevant for multi-scale systems where coupling of the sub-grid processes to the resolved processes leads to such state dependent errors [e.g. Wilks, 2005; Crommelin and Vanden-Eijnden, 2008; Arnold et al., 2013; Kwasniok, 2012]. The conditional probability density of the estimated errors given states is generated using kernel density estimation, which allows for the characterization of potentially non-Gaussian features and higher order moments which are typically ignored. Additional covariates can be included, as specific to the problem. Finally, errors sampled from the estimated conditional probability density are combined with model simulations during the assimilation phase. Error and density estimation is computed off-line (prior to undertaking data assimilation) so that the cost of incorporating uncertainty in this fashion is kept to a minimum. The procedure can be summarized by 3 basic components:

1. Offline additive error estimation
2. Conditional PDF estimation
3. Characterizing model uncertainty during assimilation

The following assumptions are required for the method:

1. The system states are directly but partially observed, i.e. \mathbf{H} takes the form as described in Section 2.
2. The additive error $\boldsymbol{\eta}_j$ is dependent on the state at the previous time \boldsymbol{x}_{j-1} , or some other collection of informative covariates. Resolving the full dependence structure between $\boldsymbol{\eta}_j$ and \boldsymbol{x}_{j-1} is generally impractical in systems with more than a few degrees of freedom. In such cases, a locality assumption is needed so that $\boldsymbol{\eta}[k]$ is dependent on states at or close to grid point k . For demonstration purposes, we will assume in the remainder of this section that $\boldsymbol{\eta}_j[k]$ is dependent on the covariate $\boldsymbol{x}_{j-1}[k]$ only. Other covariate choices are possible, and are not limited to scalars (see for example Case Study 2 in Section 4.2.1).
3. Magnitude of the measurement errors is negligible in comparison to the magnitude of the model errors, i.e. $\|\boldsymbol{\varepsilon}_j\| \ll \|\boldsymbol{\eta}_j\|$
4. Additive error statistics are the same in time and space, i.e. $\boldsymbol{\eta}_t[l] \sim p(\boldsymbol{\eta}_j[k]|\boldsymbol{x}_{j-1}[k]) \quad \forall l \in \{1, \dots, k\}, t \geq 1$

The methodology is discussed in detail for the remainder of this section.

1. Offline additive error estimation

In the following, we use the notation $\boldsymbol{\eta}_j^u$ to refer to the additive errors at time j on the unobserved variables and similarly $\boldsymbol{\eta}_j^o$ for the observed variables:

$$\boldsymbol{\eta}_j^o = \mathbf{H}\boldsymbol{\eta}_j \quad (17a)$$

$$\boldsymbol{\eta}_j^u = \mathbf{H}^\perp \boldsymbol{\eta}_j \quad (17b)$$

where $\mathbf{H}^\perp : \mathbb{R}^{N_x} \rightarrow \mathbb{R}^{N_x - N_y}$ is the orthogonal complement of \mathbf{H} . Unless otherwise stated, the notation $\mathbf{v}_{t_1:t_2}$ is used to indicate the set of vectors $\mathbf{v}_j \forall j \in \{t_1, \dots, t_2\}$. The hat notation ($\hat{\cdot}$) is used to indicate an estimate of a variable.

The goal is to estimate both $\boldsymbol{\eta}_{1:T}^o$ and $\boldsymbol{\eta}_{1:T}^u$ where T is the length of the training period. The complexity of the estimation problem can be greatly reduced by forcing the constraint that predictions match observations exactly, i.e. $\mathbf{x}_j = M(\mathbf{x}_{j-1}) + \boldsymbol{\eta}_j = \mathbf{y}_j$. This is reasonable whenever measurement noise is negligible or the magnitude of the model errors $\boldsymbol{\eta} \gg$ measurement noise $\boldsymbol{\varepsilon}$ (Assumption 3). All that is then needed is an estimate for $\boldsymbol{\eta}_{1:T}^u$ and an estimate for the initial state \mathbf{x}_0 . To see why, examine the sequence of operations for $T = 2$:

$$\hat{\boldsymbol{\eta}}_1^o = \mathbf{y}_1 - \mathbf{H}M(\hat{\mathbf{x}}_0) \quad (18a)$$

$$\hat{\boldsymbol{\eta}}_1 = \mathbf{H}^T \hat{\boldsymbol{\eta}}_1^o + [\mathbf{H}^\perp]^T \hat{\boldsymbol{\eta}}_1^u \quad (18b)$$

$$\hat{\mathbf{x}}_1 = M(\hat{\mathbf{x}}_0) + \hat{\boldsymbol{\eta}}_1 \quad (18c)$$

$$\hat{\boldsymbol{\eta}}_2^o = \mathbf{y}_2 - \mathbf{H}M(\hat{\mathbf{x}}_1) \quad (18d)$$

Note also that the additive errors are estimated at the temporal resolution

of the observations, i.e. $\boldsymbol{\eta}_j$ captures the error in transitioning from the state at time $j - 1$ to j using the model equations where observations are available at time $\{\dots, j - 1, j, j + 1, \dots\}$. Since we are dealing with an ill-posed problem, some regularizing information is needed to obtain a suitable estimate for $\boldsymbol{\eta}_{1:T}^u$. Recall that we assume $\boldsymbol{\eta}_t[l] \sim p(\boldsymbol{\eta}_j[k]|\boldsymbol{x}_{j-1}[k]) \forall l \in \{1, \dots, k\}, t \geq 1$ (Assumption 4). We have no prior information about the form of this conditional pdf (e.g. Gaussianity, unbiasedness etc.) meaning that there are several possible candidate densities. We desire a density that minimizes the total conditional variance:

$$\int Var(\boldsymbol{\eta}_j[k]|\boldsymbol{x}_{j-1}[k])d\boldsymbol{x}_{j-1}[k] \quad (19)$$

where in the above the covariate is assumed to be $\boldsymbol{x}_{j-1}[k] \in \mathbb{R}$, and the function $g(\boldsymbol{x}_{j-1}[k]) = Var(\boldsymbol{\eta}_j[k]|\boldsymbol{x}_{j-1}[k])$ is assumed to be bounded and continuous. Note also that equation 19 is not equal to the marginal variance of $\boldsymbol{\eta}_j[k]$.

The integral in equation 19 is approximated numerically via a trapezoidal rule (the following is presented for the case where the covariate is scalar but can be easily extended to the multivariate case):

$$\begin{aligned} & \int Var(\boldsymbol{\eta}_j[k]|\boldsymbol{x}_{j-1}[k])d\boldsymbol{x}_{j-1}[k] \\ & \approx \sum_{i=1}^{N_b} \frac{Var(\boldsymbol{\eta}_j[k]|\boldsymbol{x}_{j-1}[k] = a_{i-1}) + Var(\boldsymbol{\eta}_j[k]|\boldsymbol{x}_{j-1}[k] = a_i)}{2} \Delta a_i \end{aligned} \quad (20)$$

where $\{a_0, a_1, \dots, a_{N_b}\}$ is a suitably chosen partition of the interval $a_0 \leq \boldsymbol{x}_{j-1}[k] \leq a_{N_b}$ and $\Delta a_i = a_i - a_{i-1}$. Since the true function $Var(\boldsymbol{\eta}_j[k]|\boldsymbol{x}_{j-1}[k])$

is unavailable, we must obtain approximations of this function at the discrete points $\mathbf{x}_{j-1}[k] = \{a_0, a_1, \dots, a_m\}$. We use the sample variance of the additive errors for $\mathbf{x}_{j-1}[k]$ in a neighbourhood of each a_i to approximate this function (since we do not have sufficient sample points at exactly each a_i). This is detailed below.

Let $\boldsymbol{\eta}_{t_1:t_2}^*$ be a sample set of estimates for $\boldsymbol{\eta}_j$ obtained from time t_1 to t_2 and similarly $\mathbf{x}_{t_1-1:t_2-1}^*$ the sample set for the covariate \mathbf{x}_{j-1} obtained from time $t_1 - 1$ to $t_2 - 1$ using the sequence of operations as indicated in equation 18:

$$\boldsymbol{\eta}_{t_1:t_2}^* = \left[[\hat{\boldsymbol{\eta}}_{t_1}]^T, [\hat{\boldsymbol{\eta}}_{t_1+1}]^T, \dots, [\hat{\boldsymbol{\eta}}_{t_2}]^T \right]^T \in \mathbb{R}^{(N_x(t_2-t_1)) \times 1} \quad (21a)$$

$$\mathbf{x}_{t_1-1:t_2-1}^* = \left[[\hat{\mathbf{x}}_{t_1-1}]^T, [\hat{\mathbf{x}}_{t_1}]^T, \dots, [\hat{\mathbf{x}}_{t_2-1}]^T \right]^T \in \mathbb{R}^{(N_x(t_2-t_1)) \times 1} \quad (21b)$$

Let $\mathbf{v}_i \in \mathbb{R}^{N_i \times 1}$ be the vector of indices such that the corresponding elements in $\mathbf{x}_{t_1-1:t_2-1}^*$ lie in a neighbourhood of a_i :

$$\mathbf{x}_{t_1-1:t_2-1}^*[\mathbf{v}_i[l]] \in \left[a_i - \frac{\Delta a_i}{2}, a_i + \frac{\Delta a_{i+1}}{2} \right] \quad \forall l \in \{1, \dots, N_i\} \quad (22)$$

where N_i is the number of sample points lying in the neighbourhood of a_i . The integrand in equation 19 can then be approximated at a point $\mathbf{x}_{j-1}[k] = a_i$ using the sample variance:

$$\begin{aligned} \text{Var}(\boldsymbol{\eta}_j[k] | \mathbf{x}_{j-1}[k] = a_i) &\approx \Psi(\boldsymbol{\eta}_{t_1:t_2}^*, \mathbf{v}_i) \\ &:= \frac{1}{N_i - 1} \sum_{l=1}^{N_i} \left(\boldsymbol{\eta}_{t_1:t_2}^*[\mathbf{v}_i[l]] - \overline{\boldsymbol{\eta}_{t_1:t_2}^*[\mathbf{v}_i]} \right)^2 \end{aligned} \quad (23)$$

where $\bar{\mathbf{z}}$ indicates the sample mean of values in the vector \mathbf{z} .

Finally, the total conditional variance can be approximated by combining equations 19 and 23:

$$\int \text{Var}(\boldsymbol{\eta}_j[k]|\mathbf{x}_{j-1}[k])d\mathbf{x}_{j-1}[k] \approx \sum_{i=1}^{N_b} \frac{\Psi(\boldsymbol{\eta}_{t_1:t_2}^*, \mathbf{v}_{i-1}) + \Psi(\boldsymbol{\eta}_{t_1:t_2}^*, \mathbf{v}_i)}{2} \Delta a_i \quad (24)$$

so that the ultimate goal is to calculate $\hat{\boldsymbol{\eta}}_{1:T}^u$ (equivalently, $\boldsymbol{\eta}_{t_1:t_2}^*$ for $t_1 = 1, t_2 = T$) as the minimizer of equation 24.

Optimizing $\hat{\boldsymbol{\eta}}_{1:T}^u$ can be prohibitively expensive especially for large T and N_x . We therefore propose to use a sequential optimization technique over a sliding time window of length τ , as is also employed in Long window weak-constraint 4D-Var [Tremolet, 2006]. For a given time t and starting from a suitable initial condition estimate $\hat{\mathbf{x}}_{t-1}$, the idea is to optimize $\hat{\boldsymbol{\eta}}_{t:t+\tau}^u$:

$$\hat{\boldsymbol{\eta}}_{t:t+\tau}^u = \underset{\boldsymbol{\eta}_{t:t+\tau}^u}{\text{argmin}} J(\hat{\mathbf{x}}_{t-1}, \boldsymbol{\eta}_{t:t+\tau}^u) \quad (25)$$

where the function J consists of evaluating the RHS of equation 24 with \mathbf{v}_{i-1} defined according to equation 22 (as outlined in Algorithm 2). The estimate $\hat{\boldsymbol{\eta}}_t^u$ is taken to have converged (assuming τ is large enough) as it would have already been optimized $\min\{t, \tau\}$ times due to the overlapping time windows. This aspect allows one to avoid specifying the background error covariance matrix or including the initial condition $\hat{\mathbf{x}}_{t-1}$ in the optimization [Tremolet, 2006]. Hence, $\hat{\boldsymbol{\eta}}_t^u$ is used to generate the final estimate of the state $\hat{\mathbf{x}}_t^u$ using equations 18a to 18c (with time index modified as appropriate). This process

is then repeated by moving in time one sub-interval, so that the next step involves optimizing $\hat{\boldsymbol{\eta}}_{t+1:t+\tau+1}^u$, where the existing estimates from the previous optimization step are used as an initial guess to the optimizer. In this study, we adopt the well-known non-linear least squares Levenberg-Marquardt algorithm [Marquardt, 1963] as the optimization algorithm. It is necessary to consider a number of factors when choosing the optimization window τ : 1) it must not be so large that the optimization procedure is computationally infeasible; 2) it should be sufficiently large so that there are enough points to approximate the conditional variance; and 3) it should be large enough so that that inclusion of a new observation at the end of the time window does not influence the initial condition.

The full error estimation procedure is described in Algorithm 1 and 2. Additionally, a pictorial representation of the optimization over a single time window is provided in Figure 1. It shows the estimated errors at various stages of the iterative minimization process for the numerical experiment considered in Section 4.

2. Conditional PDF Estimation

The resulting sample of additive error and states estimates $\hat{\boldsymbol{\eta}}_{1:T}^u$ and $\hat{\boldsymbol{x}}_{0:T-1}^u$ is then used to derive the conditional probability density e.g. $p(\boldsymbol{\eta}_j[k]|\boldsymbol{x}_{j-1}[k])$. As mentioned earlier, it is also possible to include additional covariates that strongly influence the errors at the current time (e.g. $\boldsymbol{\eta}_{j-1}[k]$ to capture serial dependence, as demonstrated in the numerical experiments in Section 4). The set of covariates is likely to be problem dependent; prior knowledge of the system is required to select them appropriately.

Algorithm 1 Model Error Estimation over training period

1: Set:

- window size τ
- initial state $\hat{\mathbf{x}}_0$
- total time series length T
- initial guess for errors on unobserved variables $\hat{\boldsymbol{\eta}}_{1:T}^u$

2: **for** $t = 1 : T - \tau$ **do**

3: Calculate:

$$\hat{\boldsymbol{\eta}}_{t:t+\tau}^u = \underset{\boldsymbol{\eta}_{t:t+\tau}^u}{\operatorname{argmin}} J(\hat{\mathbf{x}}_{t-1}, \boldsymbol{\eta}_{t:t+\tau}^u)$$

where J is evaluated using function `EVALJ` (see Algorithm 2) and the initial guess for $\boldsymbol{\eta}_{t:t+\tau}^u$ is the current set $\hat{\boldsymbol{\eta}}_{t:t+\tau}^u$.

4: Calculate:

$$\hat{\boldsymbol{\eta}}_t^o = \mathbf{y}_t - \mathbf{H}\mathbf{M}(\hat{\mathbf{x}}_{t-1}) \tag{26a}$$

$$\hat{\boldsymbol{\eta}}_t = \mathbf{H}^T \hat{\boldsymbol{\eta}}_t^o + [\mathbf{H}^\perp]^T \hat{\boldsymbol{\eta}}_t^u \tag{26b}$$

$$\hat{\mathbf{x}}_t = \mathbf{M}(\hat{\mathbf{x}}_{t-1}) + \hat{\boldsymbol{\eta}}_t \tag{26c}$$

5: **end for**

6: **return** $\hat{\boldsymbol{\eta}}_{1:T}$; $\hat{\mathbf{x}}_{0:T-1}$

Algorithm 2 Evaluate cost function

1: **function** EVALJ ($\hat{\mathbf{x}}_{t-1}, \hat{\boldsymbol{\eta}}_{t:t+\tau}^u, \mathbf{y}, t$)
 2: **for** $l = t : t + \tau$ **do**
 3:

$$\hat{\boldsymbol{\eta}}_l^{int,o} = \mathbf{y}_l - \mathbf{H}M(\hat{\mathbf{x}}_{l-1}) \quad (27a)$$

$$\hat{\boldsymbol{\eta}}_l^{int} = \mathbf{H}^T \hat{\boldsymbol{\eta}}_l^{int,o} + [\mathbf{H}^\perp]^T \hat{\boldsymbol{\eta}}_l^u \quad (27b)$$

$$\hat{\mathbf{x}}_l = M(\hat{\mathbf{x}}_{l-1}) + \hat{\boldsymbol{\eta}}_l^{int} \quad (27c)$$

4: **end for**
 5: Set:

$$\boldsymbol{\eta}_{t:t+\tau}^* = [[\hat{\boldsymbol{\eta}}_t^{int}]^T, [\hat{\boldsymbol{\eta}}_{t+1}^{int}]^T, \dots, [\hat{\boldsymbol{\eta}}_{t+\tau}^{int}]^T]^T \quad (28a)$$

$$\mathbf{x}_{t-1:t+\tau-1}^* = [[\hat{\mathbf{x}}_{t-1}]^T, [\hat{\mathbf{x}}_t]^T, \dots, [\hat{\mathbf{x}}_{t+\tau-1}]^T]^T \quad (28b)$$

6: Define: $\{a_0, a_1, \dots, a_{N_b}\}$ where $a_0 \leq \mathbf{x}_{t-1}[k] \leq a_{N_b}$ and $\Delta a_i = a_i - a_{i-1}$
 7: **for** $l = 1 : (N_x \tau)$ **do**
 8: **for** $i = 1 : N_b$ **do**
 9: **if** $(a_i - \frac{\Delta a_i}{2}) \leq \mathbf{x}_{t-1:t+\tau-1}^*[l] \leq (a_i + \frac{\Delta a_{i+1}}{2})$ **then**
 10: $\mathbf{v}_i = [\mathbf{v}_i, l]$
 11: **end if**
 12: **end for**
 13: **end for**
 14: Calculate:

$$J = \sum_{i=1}^{N_b} \frac{\Psi(\boldsymbol{\eta}_{t:t+\tau}^*, \mathbf{v}_{i-1}) + \Psi(\boldsymbol{\eta}_{t:t+\tau}^*, \mathbf{v}_i)}{2} \Delta a_i \quad (29)$$

where Ψ is defined in equation 23

15: **return** J
 16: **end function**

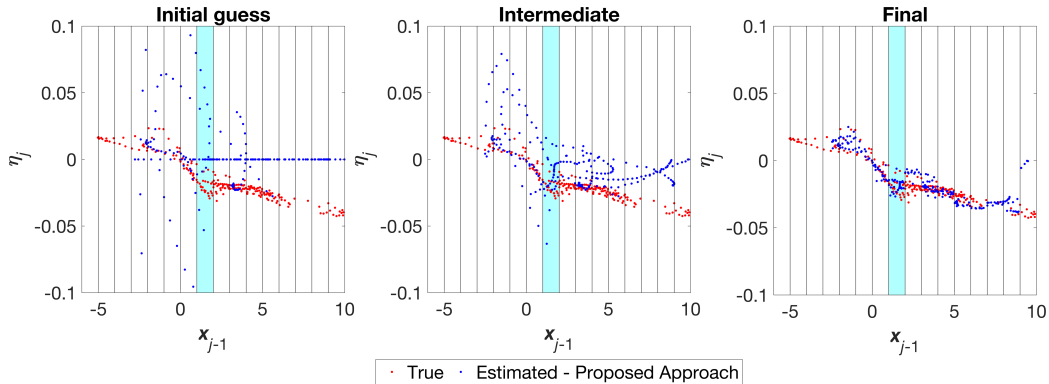


Figure 1: Representative example of the minimization process in the proposed approach for a single window. Here an iterative minimization algorithm is used and the results are shown at various stages (a - initial guess = 0 for errors on unobserved states, b - intermediate and c - final). The aim is to minimize the spread of the errors within each bin (i.e. each rectangle), subject to the constraint that the estimated states match the observations. Notice in particular how the spread of the errors in the blue highlighted rectangle gradually becomes smaller from a) to c).

For density estimation, we propose utilising nonparametric methods so as to avoid specification of a parametric distribution, which may be difficult for complex error structures. Kernel Conditional Density Estimation methods [Hyndman et al., 1996; Hall et al., 2004] are well suited to such a task, although they are generally data-intensive and suffer from the curse of dimensionality. However, they are sufficient for the class of problems considered herein where the locality assumption greatly reduces the dimension of the response variable and covariates. In this study, we adopt the method of Hayfield and Racine [2008] as implemented in the np package in R.

3. Characterizing model uncertainty during assimilation

All that remains is to sample from the estimated probability density when

undertaking ensemble filtering. Additive errors are sampled from the estimated conditional density $p(\boldsymbol{\eta}_j[k]|\mathbf{x}_{j-1}[k] = \mathbf{x}_{j-1}^{ai}[k])$ and added to the model simulations $M(\mathbf{x}_{j-1}^{ai})$ at any given time j in the assimilation period that coincides with an available observation:

$$\mathbf{x}_j^{fi} = M(\mathbf{x}_{j-1}^{ai}) + \boldsymbol{\eta}_j^i \quad \forall \quad i \in \{1, 2, \dots, n\} \quad (30)$$

where $\boldsymbol{\eta}_j^i[k] \sim p(\boldsymbol{\eta}_j[k]|\mathbf{x}_{j-1}[k] = \mathbf{x}_{j-1}^{ai}[k])$. Sampling can be undertaken using standard methods for sampling from weighted mixture distributions, where the distribution is the adopted kernel function during the density estimation phase.

We conclude this section by summarizing the key advantages over existing methods, in particular: 1) the proposed method allows for the estimation of complex state dependent error structures with minimal a priori knowledge and partial observations; 2) requires no assumptions or specification of a parametric error distribution (e.g. Gaussian errors) and considers the full range of moments (not just bias and covariance); 3) all error statistics are computed from data, without the need for numerical tuning; and 4) has sufficient flexibility to incorporate a range of covariates that influence error processes, which will generally be problem dependent.

3.2. Benchmark Methods

The stochastic parameterization methods for multi-scale systems discussed in Section 1 [Wilks, 2005; Crommelin and Vanden-Eijnden, 2008; Kwasniok, 2012; Arnold et al., 2013; Lu et al., 2017, e.g] require knowl-

edge of the sub-grid scale processes and/or fully observed resolved variables. These approaches are therefore inapplicable for the problem setting considered here. In the remainder of this section, two existing Data Assimilation based methods that are amenable to our problem setting are discussed. They are also adopted as benchmarks for comparison with the proposed approach.

3.2.1. B1 - Analysis Increment Based Method

Several researchers have investigated the potential of utilising analysis increments from a data assimilation run to characterize model errors [Leith, 1978; Li et al., 2009; Mitchell and Carrassi, 2015, see for example]. We adopt the recently proposed ETKF-TV of Mitchell and Carrassi [2015] as a representative method of such approaches (hereafter referred to as Method B1). Their method involves generating a forecast ensemble by perturbing model simulations with random noise, where the noise statistics are estimated from the analysis increments of a suitably optimized ETKF assimilation (referred to as the reanalysis assimilation run of length T):

$$\mathbf{x}_j^{fi} = M(\mathbf{x}_{j-1}^{ai}) - \alpha \boldsymbol{\eta}_j^i \quad (31)$$

$$\boldsymbol{\eta}_j^i \sim N(\bar{\mathbf{b}}_m, \bar{\mathbf{P}}_m) \quad (32)$$

where \mathbf{x}_j^{fi} = i th member of the forecast ensemble at time j ; \mathbf{x}_{j-1}^{ai} = i th member of the analysis at time $j - 1$; and α is a tuning parameter. The errors are assumed to be normally distributed with mean $\bar{\mathbf{b}}_m$ and covariance $\bar{\mathbf{P}}_m$, whose values are estimated from the analysis increments $\delta \mathbf{x}_j^a$ calculated

over the training period:

$$\delta \mathbf{x}_j^a = \frac{1}{n} \sum_{i=1}^n (\mathbf{x}_j^{ai} - \mathbf{x}_j^{fi}) \quad (33)$$

$$\bar{\mathbf{b}}_m = \frac{1}{T} \sum_{j=1}^T \delta \mathbf{x}_j^a \quad (34)$$

$$\bar{\mathbf{P}} = \frac{1}{T-1} \sum_{j=1}^T [\delta \mathbf{x}_j^a - \bar{\mathbf{b}}_m] [\delta \mathbf{x}_j^a - \bar{\mathbf{b}}_m]^T \quad (35)$$

where \mathbf{x}_j^{ai} and \mathbf{x}_j^{fi} refer to the i th ensemble member at time j obtained from the reanalysis assimilation run for the analysis and forecast respectively. Note equations 33 to 35 are derived assuming the analysis interval length is the same in the reanalysis and experimental run (as is the case in this study). Here the reanalysis run is undertaken using the ETkF with tuned multiplicative inflation [Anderson and Anderson, 1999; Hamill et al., 2001, e.g] whereby the ensemble spread is increased according to equation 36:

$$\mathbf{x}_j^{f*i} = \sqrt{\lambda} (\mathbf{x}_j^{fi} - \bar{\mathbf{x}}_j^f) + \bar{\mathbf{x}}_j^f \quad (36)$$

where λ is the tunable inflation factor usually slightly greater than 1; \mathbf{x}_j^{f*i} represents the inflated forecast ensemble member; and $\bar{\mathbf{x}}_j^f$ is the forecast ensemble mean at time j . Here the need for localization is avoided through the use of a large ensemble size (see Section 4.2).

As noted in Mitchell and Carrassi [2015], the increment -based statistics do not account for analysis errors. There is therefore the potential for over-estimation of model errors due to inaccuracies associated with the as-

simulation update. This effect is overcome through the inclusion of a tuning parameter α in equation 31 which can be optimized similar to the inflation parameter λ .

3.2.2. B2 -Error estimation using Long Window Weak Constraint 4D-VAR

As discussed in Section 3.1, the proposed method for estimation of additive errors relies on ideas from Long window weak-constraint 4D-VAR [Tremolet, 2006] to avoid specification of the background covariance matrix. However, it differs in the specification of the cost function, as the 4D-VAR method provides the least square solution for the model error control variable. It is therefore natural to compare the proposed approach to the standard Long window weak constraint 4D-VAR estimation method. Since the focus here is on the offline error estimation phase, the second benchmark (Method B2) is taken to be the same as the proposed approach, but with Step 1 (see Section 3.1) replaced by Long window weak constraint 4D-VAR. The probability density estimation (Step 2) and sampling approach (Step 3) remain unchanged. It is worth noting that this is not exactly a "standard" method in its entirety, but is investigated to examine the benefit of a specific element of the proposed method. The long window weak constraint 4D-VAR method is discussed below.

In variational data assimilation, model errors are typically accounted for using weak constraint 4D-VAR. In the formulation where the initial state and model errors are considered as control variables, this amounts to minimizing

the following cost function over a time window of length τ [Tremolet, 2006]:

$$\begin{aligned}
J(\mathbf{x}_0, \boldsymbol{\eta}) = & \underbrace{\frac{1}{2} (\mathbf{x}_0 - \mathbf{x}_b)^T \mathbf{B}^{-1} (\mathbf{x}_0 - \mathbf{x}_b)}_{J_B} + \underbrace{\frac{1}{2} \sum_{j=1}^{\tau} \boldsymbol{\eta}_j^T \mathbf{Q}_j^{-1} \boldsymbol{\eta}_j}_{J_Q} \\
& + \underbrace{\frac{1}{2} \sum_{j=0}^{\tau} (\mathbf{H}\mathbf{x}_j - \mathbf{y}_j)^T \mathbf{R}^{-1} (\mathbf{H}\mathbf{x}_j - \mathbf{y}_j)}_{J_O}
\end{aligned} \tag{37}$$

where \mathbf{x}_b is the background estimate of the initial state \mathbf{x}_0 ; \mathbf{B} is the background error covariance matrix associated with \mathbf{x}_b ; \mathbf{Q} is the model error noise covariance matrix; and $\mathbf{x}_j = M(\mathbf{x}_{j-1}) + \boldsymbol{\eta}_j$ for $j \in \{1, \tau\}$. The assimilation cycle is repeated by then considering the next assimilation window $\{\tau+1, 2\tau\}$. However, in the long window approach, minimization is performed by shifting the interval by one observation interval rather than the full assimilation window of length τ . This allows one to neglect the background term J_B from the cost function after a suitable warm up period. The estimate \mathbf{x}_b would have already converged due to the many iterations of the minimisation algorithm from the overlapping windows, meaning its uncertainty is negligible in comparison to the other terms. The window length should also be chosen to be sufficiently long, such that the inclusion of a new observation at the end of the time window does not affect the initial state (this is relevant for the proposed approach also).

In summary, the B2 method is defined as being the same as the proposed approach, but with the cost function in equation 25 replaced by minimization

of the following cost function for any given time t :

$$J(\boldsymbol{\eta}_{t:t+\tau}, \hat{\boldsymbol{x}}_{t-1}) = \underbrace{\frac{1}{2} \sum_{j=t}^{t+\tau} \boldsymbol{\eta}_j^T \mathbf{Q}_j^{-1} \boldsymbol{\eta}_j}_{J_Q} + \underbrace{\frac{1}{2} \sum_{j=t}^{t+\tau} (\mathbf{H}\boldsymbol{x}_j - \boldsymbol{y}_j)^T \mathbf{R}^{-1} (\mathbf{H}\boldsymbol{x}_j - \boldsymbol{y}_j)}_{J_O} \quad (38)$$

where $\boldsymbol{x}_j = M(\boldsymbol{x}_{j-1}) + \boldsymbol{\eta}_j$ for $j \in \{t, t + \tau\}$ and the initial condition is given by $\hat{\boldsymbol{x}}_{t-1}$.

The Levenberg-Marquardt algorithm is again used as the minimizer, for the sake of comparison with the proposed approach. Notice that unlike the proposed approach, the errors in the entire state vector (not just unobserved states) must be optimized.

4. Numerical Experiments

4.1. Multi-Scale Lorenz 96

Here we investigate the efficacy of the proposed method and benchmarks discussed in Section 3 through synthetic experiments using the multi-scale Lorenz 96 model. This system has been used extensively as a toy model of the atmosphere to test new algorithms and to study model errors due to unresolved sub-grid processes. Such toy models serve as a valuable testbed as methods can be evaluated against the truth and they are computationally inexpensive. The Lorenz 96 model was originally developed to represent mid-latitude weather evolving at a range of spatio-temporal scales. It consists of a coupled system of equations representing the evolution of an atmospheric

quantity discretized over a latitude circle at different scales:

$$\frac{dX_k}{dt} = -X_{k-1}(X_{k-2} - X_{k+1}) - X_k + F + \frac{h_x}{L} \sum_{l=1}^L Z_{l,k}; \quad k \in \{1, \dots, N_x\} \quad (39)$$

$$\frac{dZ_{l,k}}{dt} = \frac{1}{\xi} (-Z_{l+1,k}(Z_{l+2,k} - Z_{l-1,k}) - Z_{l,k} + h_z X_k); \quad l \in \{1, \dots, N_z\} \quad (40)$$

The $\{X_k\}_{k=1}^k$ slow variables represent quantities evolving on a coarse spatial scale with low-frequency large amplitude fluctuations, where the subscript k refers to the k th grid point on the latitude circle. Each X_k variable is coupled to L small-scale variables $Z_{l,k}$ that are characterized by high frequency and relatively small amplitude temporal evolution. The variables are driven by a quadratic term that models advection, a linear damping, constant forcing (F) and coupling term that links the two scales. The system is subject to periodic boundary conditions, so that $X_k = X_{k+k}$, $Z_{l,k} = Z_{l,k+k}$ and $Z_{l+L,k} = Z_{l,k+1}$. The effect of the unresolved fast variables on the slow variables is denoted by the so-called sub-grid tendency U_k :

$$U_k = \frac{h_x}{L} \sum_{l=1}^L Z_{l,k} \quad (41)$$

We use the formulation of the Lorenz 96 (equations 39 to 40) as provided in [Fatkullin and Vanden-Eijnden, 2004] which makes the time-scale separation between the slow and fast variables (measured by ξ) explicit. Note that this formulation is equivalent to the system originally proposed by Lorenz with the following variable scaling and parameter conversions: $X_k = X_k^*$ and $Z_{l,k} = Z_{l,k}^*$ where X_k^* and $Z_{l,k}^*$ are the slow and fast variables respectively in the original system; $\xi = \frac{1}{c}$ where $c =$ time scale ratio; $h_x = \frac{-hcN_z}{b^2}$ where $b =$

spatial scale ratio and h is the coupling constant; and $h_z = h$.

The behaviour of the system can vary considerably depending on the values assigned to the parameters in equations 39 to 40. Here, we consider a range of dynamical regimes so as to study the robustness of the proposed approach to different model error structures (summarised in Table 1). We first consider a case with large time scale separation ($\xi \approx 0.008$) studied by Fatkullin and Vanden-Eijnden [2004]. The sub-grid tendency has a complex non-linear dependence on the resolved variable, making it of interest to this study. However, such large time scale separations are not representative of the real atmosphere. We therefore consider a second case that has a smaller time scale separation ($\xi \approx 0.7$) and stronger coupling ($h_x = -2$) than cases considered in previous studies (where ξ is typically 0.4 or 0.5 and $h_x = 1$) [e.g. Crommelin and Vanden-Eijnden, 2008; Arnold et al., 2013; Lu et al., 2017]. Smaller values of ξ (i.e. larger time scale separation) are generally considered more difficult to parameterize, and the larger magnitude of the coupling term amplifies the effect of model errors. In both case studies, the dynamics are chaotic and give rise to complex non-Gaussian conditional error densities, as shown by the variation of U_k with X_k in Figure 2.

	Parameter	Case Study 1	Case Study 2
Lorenz 96 parameters	ξ	$\frac{1}{128} \approx 0.008$	0.7
	h_x	-0.8	-2
	h_z	1	1
	N_z	128	20
	N_x	9	9
	F	10	14
Observation density	Observation frequency (MTU)	0.02	0.04
	Location of Observed X_k	[3, 4, 8, 9]	[1, 2, 5, 6]

Table 1: Multi-scale Lorenz 96 parameters for the 2 different case studies. Note that $1\text{MTU} = \frac{1}{\Delta t}$ time steps and the model equations are discretized with $\Delta t = 8 \times 10^{-4}$.

4.2. Experimental Setup

The available forecast model is the single scale Lorenz 96 model (equation 42), where the forcing term is known perfectly but knowledge of the sub-grid processes $Z_{l,k}$ is unavailable:

$$\frac{dX_k}{dt} = -X_{k-1}(X_{k-2} - X_{k+1}) - X_k + F; \quad k \in \{1, \dots, N_x\} \quad (42)$$

Our aim is to characterize the uncertainty in model simulations due to missing physics, where the resolved variables are partially observed. The effects of uncertainty characterization on forecasts and assimilation are also of interest. Experiments proceed in two stages: 1) An error estimation phase whereby the proposed approach and benchmark methods described in Section 3 are applied to obtain estimates of model errors; and 2) An assimilation phase where these error estimates are utilized in an assimilation experiment to determine the effects on forecasts and analyses. These are discussed in

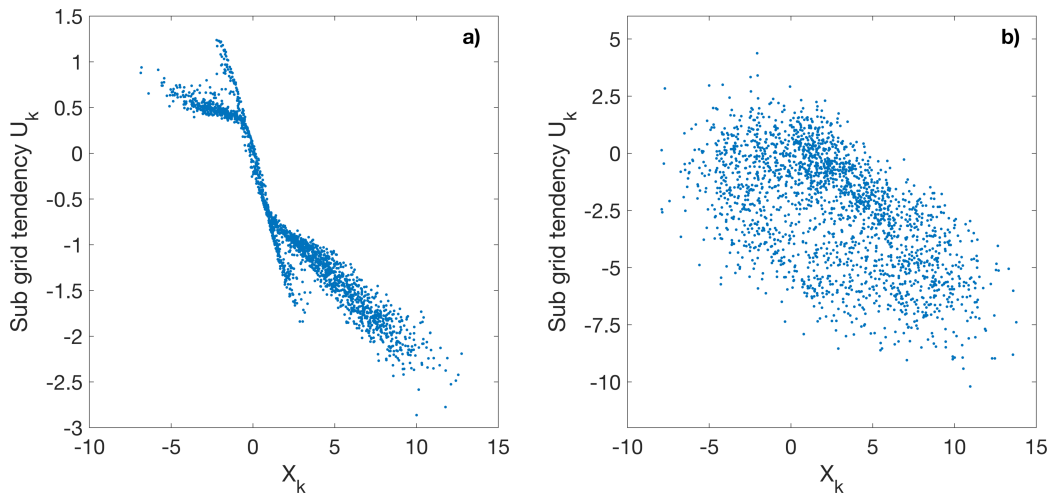


Figure 2: Sub-grid tendencies for the two different regimes of the multi-scale Lorenz 96 system considered in this study: a) Case 1 - large time scale separation; b) Case 2 - small time scale separation. For both cases, points are sampled at an interval of 0.3 MTU

detail below.

4.2.1. Training Period

A training period was designed in order to estimate the conditional error density in the proposed approach and Method B2, as well as the analysis increment statistics in Method B1. A truth run for the training period was generated by first numerically integrating the full multi-scale system (i.e. equations 39 to 40) using a fourth-order Runge-kutta scheme with adaptive time-stepping and maximum time step of $\Delta t = 0.0008$ for 820 Model Time Units (MTU), or approximately 11 years (after excluding transients). Note that $1\text{MTU} = \frac{1}{\Delta t}$ time steps. Partial observations of the resolved slow variables were then developed by perturbing the true values with zero mean,

temporally and spatially uncorrelated Gaussian noise:

$$\begin{aligned}\mathbf{y}_j &= \mathbf{H}\mathbf{x}_j + \boldsymbol{\varepsilon}_j \\ \boldsymbol{\varepsilon}_j &\sim N(0, \mathbf{R})\end{aligned}\tag{43}$$

where \mathbf{H} is a non-square matrix of 1s and 0s with $N_y < N_x$, \mathbf{x}_j is the true state at time j where $\mathbf{x}_j[k]$ is equivalent to the time discretised value of X_k in equation 39, and \mathbf{R} is a diagonal matrix with 10^{-6} on the main diagonal. \mathbf{R} is chosen such that instrument errors are negligible in comparison to model errors. The resolved variables are partially observed in space in all experiments (approx. 50% observed, refer 1), and observations are available at 0.02 and 0.04 MTU for Case Studies 1 and 2 respectively (i.e. 25 and 50 time steps). Based on the work of Lorenz [2006], this corresponds to an observation interval of 2.5 and 5 hrs respectively (1 MTU is approximately equivalent to 5 days). These interval lengths were chosen to reflect a realistic observation network whilst also maintaining complex non-Gaussian error structures.

The proposed approach was then applied to the training data, using only partial observations, perfect knowledge of the forcing F and observation error covariance \mathbf{R} , and the forecast model given in equation 42. The forecast model was integrated using a time step of $\Delta t = 8 \times 10^{-4}$. A key component of the proposed approach is the binning procedure, whereby the error estimates are grouped and the variance computed for each bin. Recall that the errors are binned according to the spatial covariates that are deemed to influence the error process. In Case Study 1, binning occurs according to $\mathbf{x}_{j-1}[k]$, whilst

a slightly more complex setup is invoked in Case study 2 where binning occurs in 2 dimensions according to $\mathbf{x}_{j-1}[k]$ and $\mathbf{x}_{j-1}[k-1]$. The parameter setting of the multi-scale Lorenz 96 in Case Study 2 is such that $\mathbf{x}_{j-1}[k-1]$ strongly influences error estimates at the neighbouring grid point $\boldsymbol{\eta}_j[k]$. Finally, additional covariates were included for Case Study 2 due to the presence of time correlations in errors in the Lorenz 96 system (as identified by e.g. Arnold et al. [2013]). In addition to the spatial covariates, error estimates at the previous time were also included, so that the final probability densities to be estimated in each case study are:

$$\text{Case Study 1: } p(\boldsymbol{\eta}_j[k]|\mathbf{x}_{j-1}[k])$$

$$\text{Case Study 2: } p(\boldsymbol{\eta}_j[k]|\mathbf{x}_{j-1}[k], \mathbf{x}_{j-1}[k-1], \boldsymbol{\eta}_{j-1}[k])$$

In a real system, such choices would be informed by expert knowledge of the error processes. Window lengths of $\tau = 25$ and 50 observation intervals (i.e. 0.5 and 2 MTU) were selected for Case Study 1 and 2 respectively. This was sufficiently long to capture a range of dynamical states and also longer than the system decorrelation time, so that the sliding window approach can be utilized to ignore the background term in the cost function (as discussed in Section 3.2.2). Data for the nonparametric conditional density estimation was generated by sampling the estimated error and states at an interval of 0.3 MTU (where autocorrelation is approximately zero, to ensure temporal independence). To avoid issues related to bandwidth specification and data sparsity in high dimensions, outlier points in the covariate space were removed from the data used for density estimation in Case Study 2.

The training data was also utilized in determining model error estimates using the benchmark methods. The same window length, optimizing algo-

rithm and density estimation algorithm used for the proposed approach was used for Method B2. Both the process and observation error covariance matrices \mathbf{Q} and \mathbf{R} were assumed to be known perfectly when evaluating equation 38 in Method B2. The process error covariance matrix was estimated by calculating the sample covariance of the true errors over the training period. For the B1 method, the ETKF was applied with additive inflation to the training data to tune the inflation parameter λ and the correction factor α . The inflation parameter was tuned based on the analysis RMSE, whilst the correction factor was selected by evaluating the spread vs RMSE relationships, as it has a greater impact on ensemble spread than accuracy. Note that localization was not required due to the large ensemble size ($n = 1000$) relative to the state dimension.

4.2.2. Assimilation Period

The estimated errors and analysis increments were then utilised in assimilation experiments and the quality of forecasts and analyses compared. Experimental conditions were kept consistent with the training period where applicable. The forecast model in the assimilation experiment was also the single scale Lorenz 96 (equation 42); spatio-temporal observation frequency was the same and observations were generated also using equation 43. Assimilation was undertaken for 30 independent runs of length 100 observation intervals with independent initial conditions. Truth runs were first generated using the same approach as for the training period. The initial conditions were generated by selecting 30 values on the attractor at intervals of 10 MTU, which is sufficient to ensure autocorrelation in the resolved variables is close to zero (also adopted by Arnold et al. [2013]). The assimilation algorithm

was the ETKF (Section 2.1) and the assimilation interval equal to the observation interval (i.e. 0.02 and 0.04 MTU for Case Study 1 and 2 respectively). Perfect initial conditions were adopted in all experiments as the focus is on the effects of model error. Similarly, a large ensemble size ($n = 1000$) was adopted to minimize the effects of sampling error and to avoid the use of localization methods. The background/prior ensemble during a single assimilation cycle at a given time j proceeds as follows:

1. Compute the model simulation for each ensemble member:

$$\mathbf{x}_j^i = M(\mathbf{x}_{j-1}^{ai}) \quad \forall \quad i \in \{1, \dots, n\} \quad (44)$$

2. Sample n values of the additive model error $\boldsymbol{\eta}_j^i$ from the probability densities estimated during the training period. For the Proposed Approach and B2 Method, this involves sampling from the non-parametrically estimated conditional density, e.g. in Case Study 1, this would be:

$$\boldsymbol{\eta}_j^i[k] \sim p(\boldsymbol{\eta}_j[k] | \mathbf{x}_{j-1}[k] = \mathbf{x}_{j-1}^i[k]) \quad \forall \quad k \in \{1, \dots, N_x\} \quad (45)$$

For the B1 Method, error estimates are sampled according to $\boldsymbol{\eta}_j^i \sim N(\bar{\mathbf{b}}_m, \bar{\mathbf{P}}_m)$

3. Generate the forecast ensemble:

$$\mathbf{x}_j^{fi} = \mathbf{x}_j^i + \boldsymbol{\eta}_t^i \quad \forall \quad i \in \{1, \dots, n\} \quad (46)$$

4.3. Results and Discussion

4.3.1. Model Error Estimation

In both case studies, the proposed approach recovers the true error estimates from partial observations more accurately than the benchmark methods. This is demonstrated qualitatively in Figure 3, which shows the sample set of additive errors $\boldsymbol{\eta}_j[k]$ against the spatial covariates (resolved variable at the previous observation time, $\boldsymbol{x}_{j-1}[k]$ for Case Study 1; and $\boldsymbol{x}_{j-1}[k-1]$ and $\boldsymbol{x}_{j-1}[k]$ for Case Study 2). In Case Study 1, the B2 method manages to at least partially recover the non-linear relationship between $\boldsymbol{\eta}_j[k]$ and $\boldsymbol{x}_{j-1}[k]$, but is less precise than estimates from the proposed method (compare Figure 3b & c). In Case Study 2, it more closely reflects the true error structure, although an overestimation and underestimation of error values is apparent in key regions of the covariate space (compare Figure 3e, f & g). Method B1 produces poor quality error estimates in both case studies; errors are grossly overestimated and the dependence structure between the errors and covariates is poorly represented. The efficacy of the three approaches in recovering the true model error statistics is quantified using the Kullback-Leibler divergence (KLD). The KLD is a measure of the difference between two probability density functions (PDF), $p(z)$ and $q(z)$ given by:

$$KLD(p, q) = \int p(z) \ln \frac{p(z)}{q(z)} dz \quad (47)$$

Lower values of the KLD indicate greater similarity between the two PDFs. For the purposes of calculating the KLD, the joint densities $p(\boldsymbol{\eta}_j[k], \boldsymbol{x}_{j-1}[k])$ and $p(\boldsymbol{\eta}_j[k], \boldsymbol{x}_{j-1}[k], \boldsymbol{x}_{j-1}[k-1])$ are estimated nonparametrically for Case

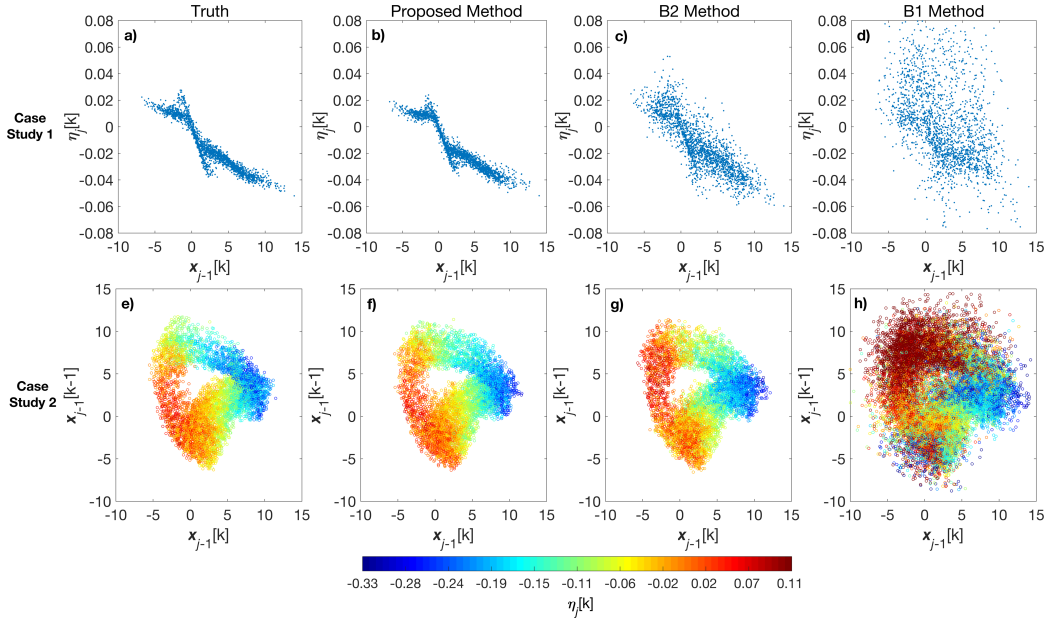


Figure 3: Sub-grid tendencies for the two different regimes of the multi-scale Lorenz 96 system considered in this study: a) to d) Case 1 - large time scale separation; b) to h) Case 2 - small time scale separation. For both cases, points are sampled at an interval of 0.3 MTU

study 1 and 2 respectively. The true density is also evaluated non-parametrically, where the sample points are given by the true errors and states. Table 2 clearly demonstrates the superiority of the proposed approach over the benchmark methods.

The model error estimation techniques considered here can also be considered as parameterizations of the sub-grid dynamics. The ability of the methods to replicate key characteristics of the full Lorenz 96 model when used in this manner is also assessed. To this end, a time series of length 10^5 data points is created where at any given time, the time discretized single layer Lorenz 96 is evaluated and combined with a single realization of

	Case Study 1 $p(\boldsymbol{\eta}_j[k], \mathbf{x}_{j-1}[k])$	Case Study 2 $p(\boldsymbol{\eta}_j[k], \mathbf{x}_{j-1}[k], \mathbf{x}_{j-1}[k-1])$
Proposed	0.14	0.34
Method B2	6.39	1.63
Method B1	78.14	12.64

Table 2: Kullback-Leibler Divergence (KLD) statistic for the estimated joint densities. The reference density is the kernel density estimate (KDE) fitted to the true sample data. Lower values of the KLD indicate that the estimated density more closely matches the reference density (reference density = KDE fitted to true error data). Note that this density is not utilised in Method B1, and is provided purely for comparison purposes.

the model error. The model error estimates apply to an interval spacing of 0.02 and 0.04 MTU for Case Study 1 and 2 respectively, so that the single layer Lorenz 96 is integrated with $\Delta t = 8 \times 10^{-4}$ within the interval. We calculate the autocorrelation function (ACF) of X_k , the cross-correlation function (CCF) between X_k and X_{k+1} , and the marginal probability density of X_k (see Figure 4). The correlation functions approximate the dynamical transitions of the slow variables whilst the marginal probability density approximates the invariant measure. Again, Method B1 performs poorly in all aspects, particularly in Case Study 2 where temporal correlations are not reproduced, meaning that the dynamical transitions are poorly represented. The results are similar to those from using inflation and localization only, in case studies with a similar time scale separation [e.g Lu et al., 2017]. The Proposed Method reproduces all three features relatively accurately in both case studies, and compares favourably with other methods that rely on data of the sub-grid processes (c.f. ACFs, CCFs and PDFs in Crommelin and Vanden-Eijnden [2008] and Lu et al. [2017]). Improvements over Method B2 are more distinct in Case Study 1 than in Case Study 2, due largely to the relatively greater similarity in error estimates in this case study (see Figure

3).

The superior performance of the proposed method is attributed to two aspects 1) the formulation of the cost function which aims to minimize the conditional variance of the estimated errors depending on the state at the previous time; and 2) optimization of errors over a time window (as is performed in traditional 4D-VAR and smoothing methods). Firstly, minimizing the conditional variance of the errors allows one to estimate more complex state dependent error structures, as opposed to the 4D-VAR type approach in Method B2 where the aim is to minimize the sum of squared errors regardless of the state of the system. The error estimates from Method B2 give J_Q terms (see equation 38) that are most often lower than J_Q of the true data (see Figure 5), meaning that estimates are obtained by minimizing an inappropriate cost function for this setting. Furthermore, the proposed approach has the added benefit of avoiding the specification of a model noise covariance matrix, which is needed in Method B2. We also undertook experiments where errors are estimated by a pure minimization of sum of squares approach, under the constraint that model predictions match observations perfectly. This approach is identical to Method B2, but using the following cost function:

$$J(\boldsymbol{\eta}_{t:t+\tau}^u, \hat{\boldsymbol{x}}_{t-1}) = \sum_{j=t}^{t+\tau} (\hat{\boldsymbol{\eta}}_j^{int})^T \hat{\boldsymbol{\eta}}_j^{int} \quad (48)$$

where $\hat{\boldsymbol{\eta}}_j^{int}$ is obtained through the operations in equation 27. This approach gave similar results to that of Method B2 for both case studies, indicating that the conditional variance cost function is critical to the improved perfor-

mance of the proposed approach.

Secondly, optimization over a time window allows one to more effectively constrain the range of possible errors in the partially observed setting, particularly when errors are time correlated. This partly explains the poor performance of Method B1 (which is based on increments from a filter) relative to the proposed approach and Method B2 which both utilize this strategy. Furthermore, the error estimates from Method B1 are heavily influenced by the quality of the assimilation algorithm (here ETKF with inflation). Poorly specified prior uncertainty in the unobserved variables from the inflation procedure can lead to large incremental updates in observed variables at future times. This ultimately corrupts the error estimates, as the increments are now dominated by initial condition errors in the unobserved variables.

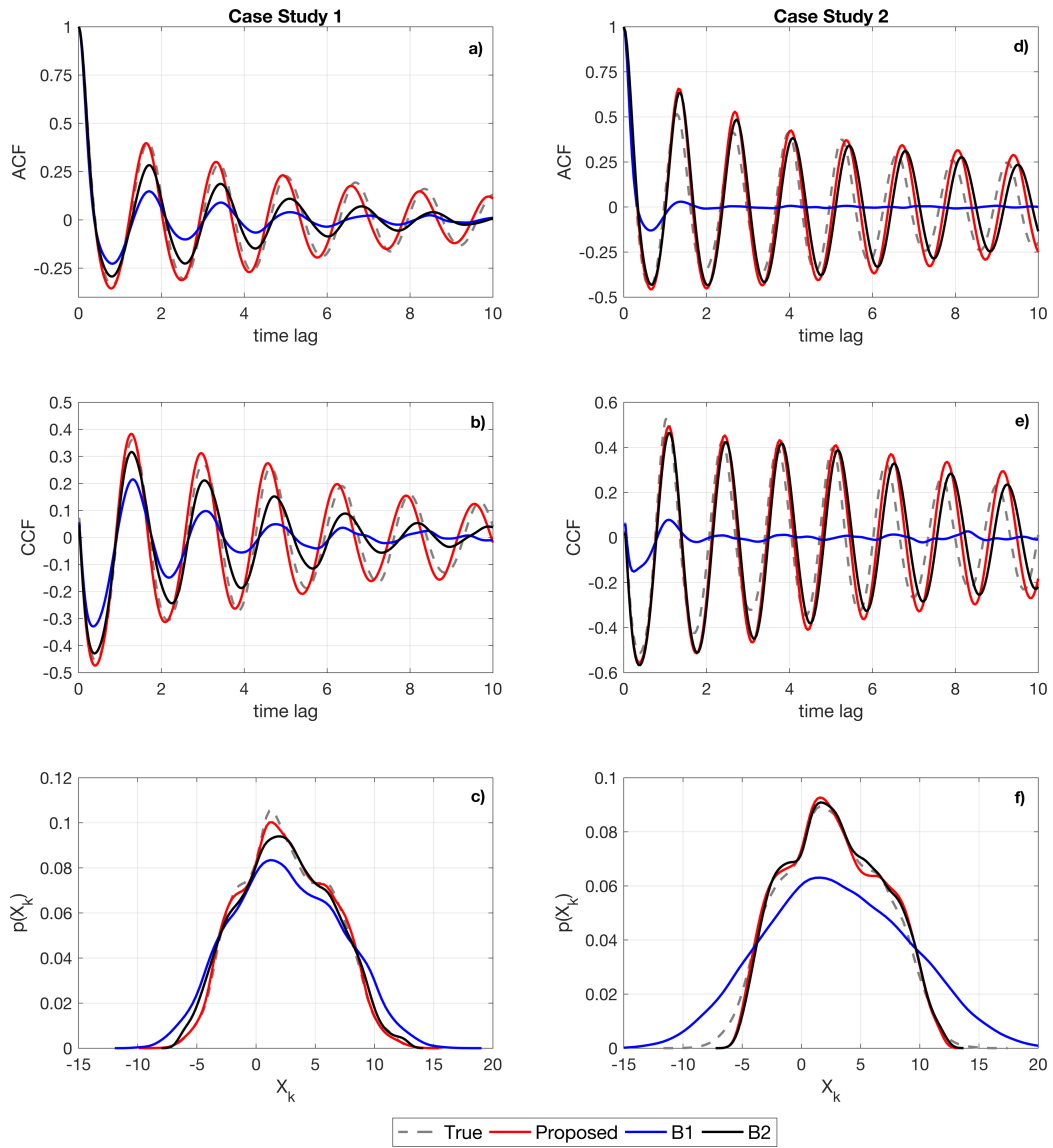


Figure 4: ACF, CCF and marginal density of a resolved variable for both case studies using different parameterization approaches.

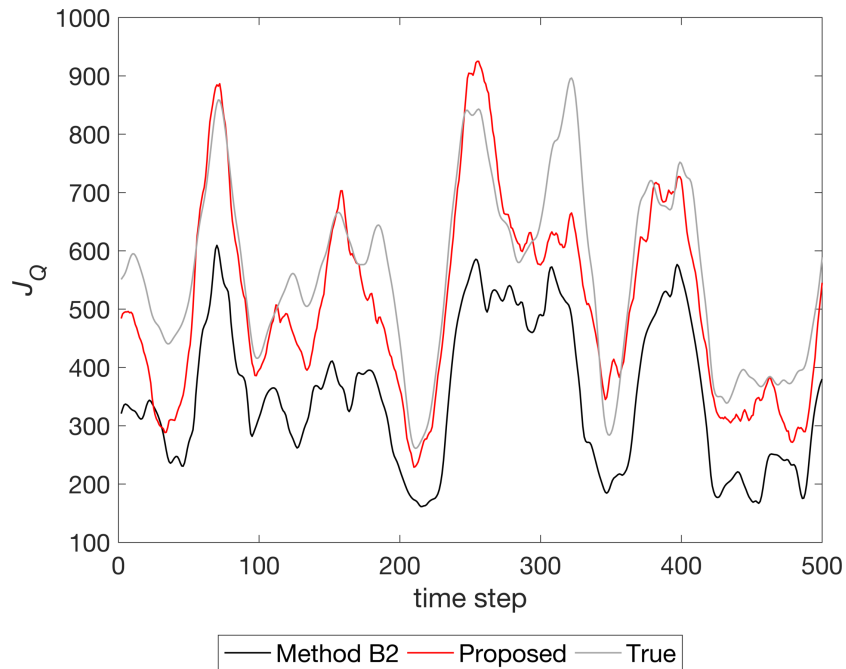


Figure 5: Snapshot of J_Q values (see Equation 38) for method B2, proposed and the true data for Case Study 2.

4.3.2. Forecast Skill

The superior error estimates from the proposed approach leads to improved forecasts compared to the benchmark methods. Representative results of one-step-ahead forecasts for both case studies are provided in Figure 6 and Figure 7. They show the forecast probability density function (pdf) of the ensemble anomalies (forecast - truth) for both an observed (left column) and unobserved variable (right column) for a single assimilation run of 100 cycles. In both case studies, relatively large systematic errors can be seen when using Method B1 compared to the other approaches, which is unsurprising given the results in Figure 3. One step ahead forecasts of the observed variables are relatively similar between the proposed method and the B2

method, although the forecast variance is considerably lower, particularly in Case Study 1. This is a direct consequence of the more precise additive model error estimates obtained from the proposed approach. For instance, resolving bimodality of the transition errors allows one to generate more accurate analyses (hence initial conditions for subsequent time steps) and forecasts even in an Ensemble Kalman Filter setting. This is demonstrated in Figure 8 where initial conditions and forecasts in Method B2 have greater variance than in the proposed method, as it is unable to precisely resolve the two modes of the error density. Differences between forecasts from the proposed and B2 method are much more pronounced for the hidden variables, where both bias and variance are much lower when using the proposed method in both case studies. The conditional variance minimization procedure allows for a more accurate representation of the spatial dependence structure. This means that information from observed variables is more effectively transferred to unobserved variables during the assimilation, thereby contributing to the improved forecasts seen for the Proposed Method compared to Method B2, through better initial conditions. Forecast skill is assessed quantitatively in the remainder of this section.

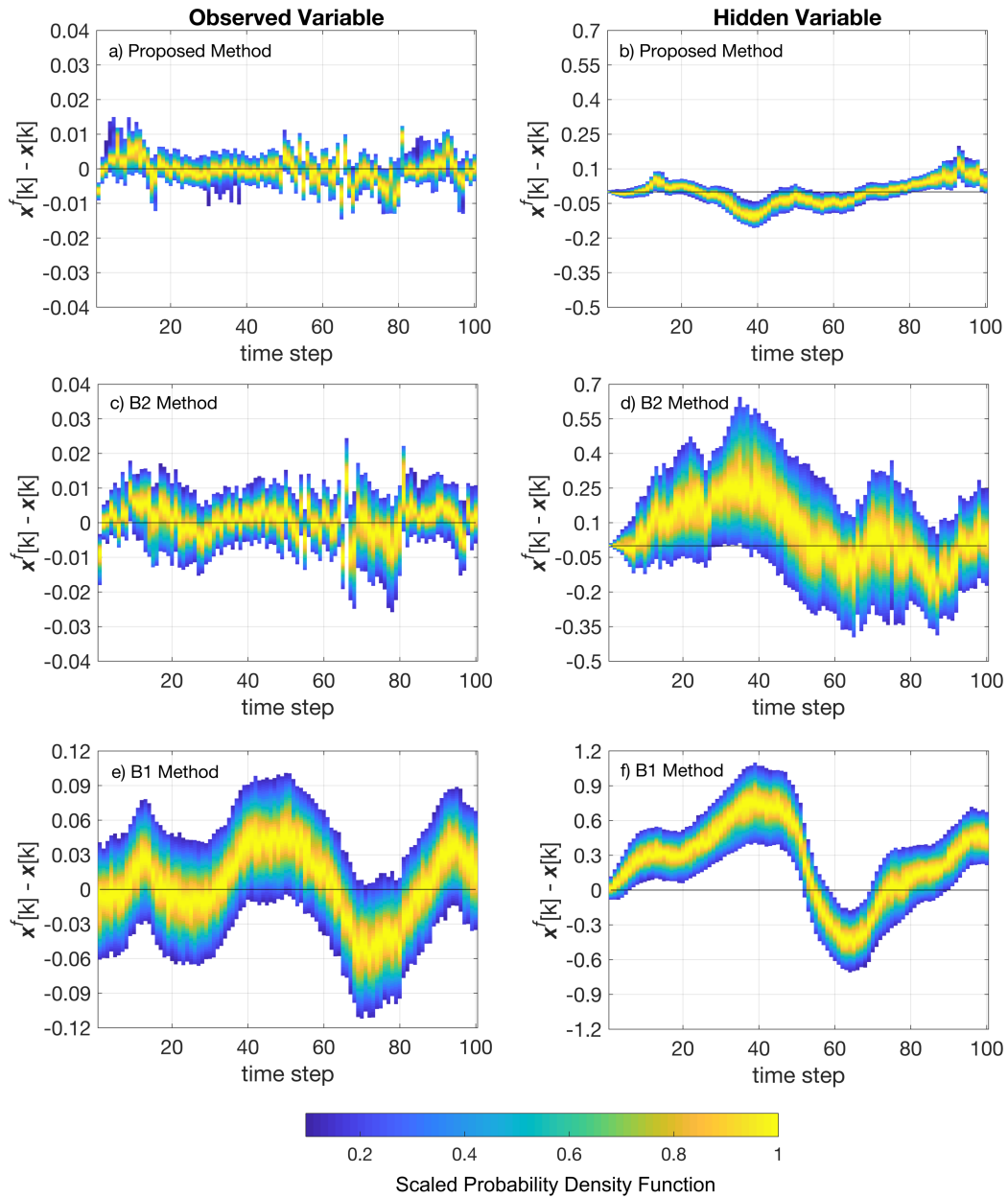


Figure 6: Representative forecast probability densities of anomalies ($x_t^f[k] - x_t[k]$) for an observed variable (left column) and unobserved variable (right column) for the different methods for Case Study 1. Forecasts are one-step-ahead (in this case, 0.02 MTU).

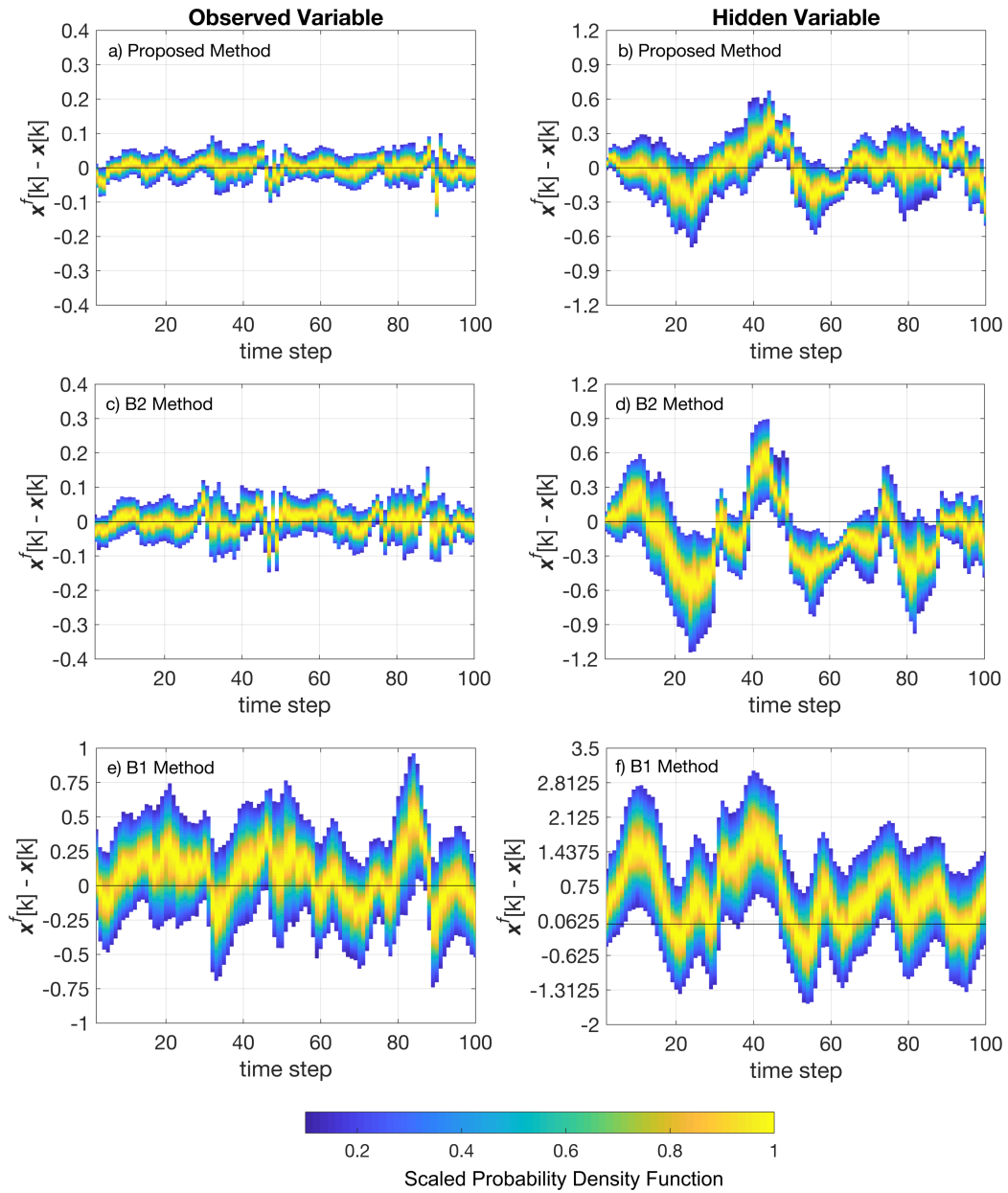


Figure 7: Representative forecast probability densities of anomalies ($x_t^f[k] - x_t[k]$) for an observed variable (left column) and unobserved variable (right column) for the different methods for Case Study 2. Forecasts are one-step-ahead (in this case, 0.04 MTU).

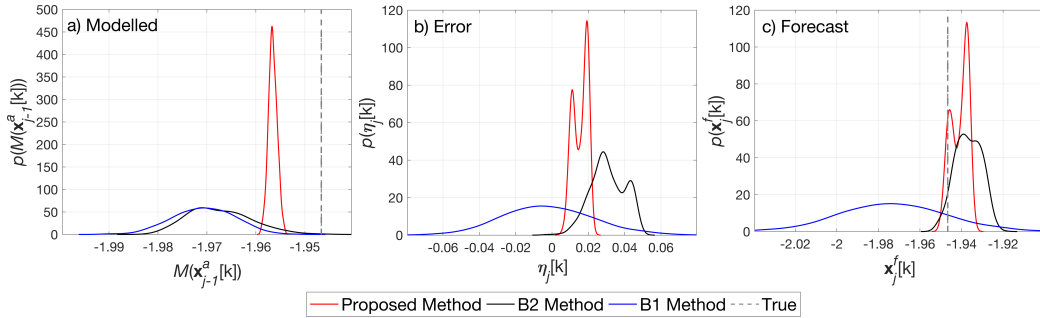


Figure 8: Example showing benefit of accounting for bimodal transition in an observed variable in Case Study 1 (shown for $t = 82$ in Figure 6)

A range of forecast metrics were considered to quantify forecast properties including reliability, resolution, accuracy and consistency. Reliability and resolution were quantified using the Continuous Ranked Probability Score (CRPS) and (negative) Logarithmic Score (LS) given in equations 49 to 51:

$$CRPS_j = \int_{-\infty}^{\infty} \left(F_j^f(y) - F_j^o(y) \right)^2 dy \quad (49)$$

$$F_j^o(y) = \begin{cases} 0 & y < y_j \\ 1 & y \geq y_j \end{cases} \quad (50)$$

$$LS_j = -\ln \left(p_j^f(y = y_j) \right) \quad (51)$$

where $F_j^f(y)$ is the empirical cumulative distribution function of the forecast of variable y at time j ; $F_j^o(y)$ is the cumulative distribution function of the observations of y at time j ; and $p_j^f(y = y_j)$ indicates the value of the forecast probability density function, evaluated at the observation value. For cases where only a single observation of y is available at each time, the Heaviside step function is used to characterize the cumulative distribution function of

the observation (see equation 50).

The CRPS is routinely adopted in forecasting studies, although it can be a poor statistic for complex forecast probability densities (see for example Smith et al. [2015] who showed that the CRPS can give misleadingly good scores to outcomes that fall in between two modes of a bimodal forecast density). Hence the LS is also calculated, although it has the drawback of heavily penalising forecasts in which the outcome falls outside the forecast range. Accuracy is measured by the Root Mean Squared Error (RMSE), which is evaluated on the ensemble mean. Finally, statistical consistency is characterized using RMS Error vs. RMS Spread diagnostic plots, which has been adopted in similar studies [see e.g. Arnold et al., 2013]. Ensemble forecasts are considered statistically consistent if the expected ensemble variance equals the expected squared ensemble mean error (assuming unbiasedness and a large enough ensemble size), where the expectation is generally evaluated over discrete bins. Here, forecasts are separated into 10 equally populated bins according to their forecast variance, and the mean square spread and mean square error are calculated for each bin prior to taking the square root. Finally, the concept of the forecast skill score (FSS) was utilized to quantify the relative improvement of the proposed approach over the benchmark methods, defined as:

$$FSS = \frac{Score_{Pr} - Score_{Be}}{Score_{Pe} - Score_{Be}} \quad (52)$$

where $Score_{Pr}$ indicates the forecast score of the proposed method; $Score_{Be}$ indicates the forecast score of the reference method (i.e. Method B1 or B2);

and $Score_{Pe}$ indicates the score associated to a perfect forecast (e.g. a perfect forecast has $CRPS = 0$). A skill score of 0.5 means that the proposed approach provides a 50% improvement over the benchmark, whilst a negative score indicates a degradation in performance.

Overall, the proposed method was found to outperform the benchmark methods in all forecast metrics considered across a range of lead times, in both case studies. This is demonstrated in Figure 9 which shows the space and time averaged forecast score against lead time. Forecasts from the proposed approach have better reliability, resolution and accuracy scores than the benchmarks, and are significantly more skilful at longer lead times (e.g. 0.6 MTU, or approximately 3 days). The observed improvements are robust to different dynamical regimes, as indicated in Figure 10 which shows the mean and standard deviation of skill scores computed over the 30 independent simulations. Relative improvements are greatest when comparing to Method B1, where the proposed approach offers a 70% improvement on average based on the RMSE and CRPS, although a sizeable improvement of 30% is still apparent when comparing to Method B2 in Case Study 2 (see Figure 10). The less pronounced improvement in terms of the LS in both case studies is attributed to the large penalty associated with forecasts where the outcome falls outside the ensemble range (regardless of the distance from the ensemble), which has a tendency to occur more frequently than in the benchmark methods. However, forecast ensembles from the proposed approach have better consistency properties, as shown by the RMS Error vs RMS Spread diagnostic plots (Figure 11) where the points lie closer to the

diagonal in the proposed approach.

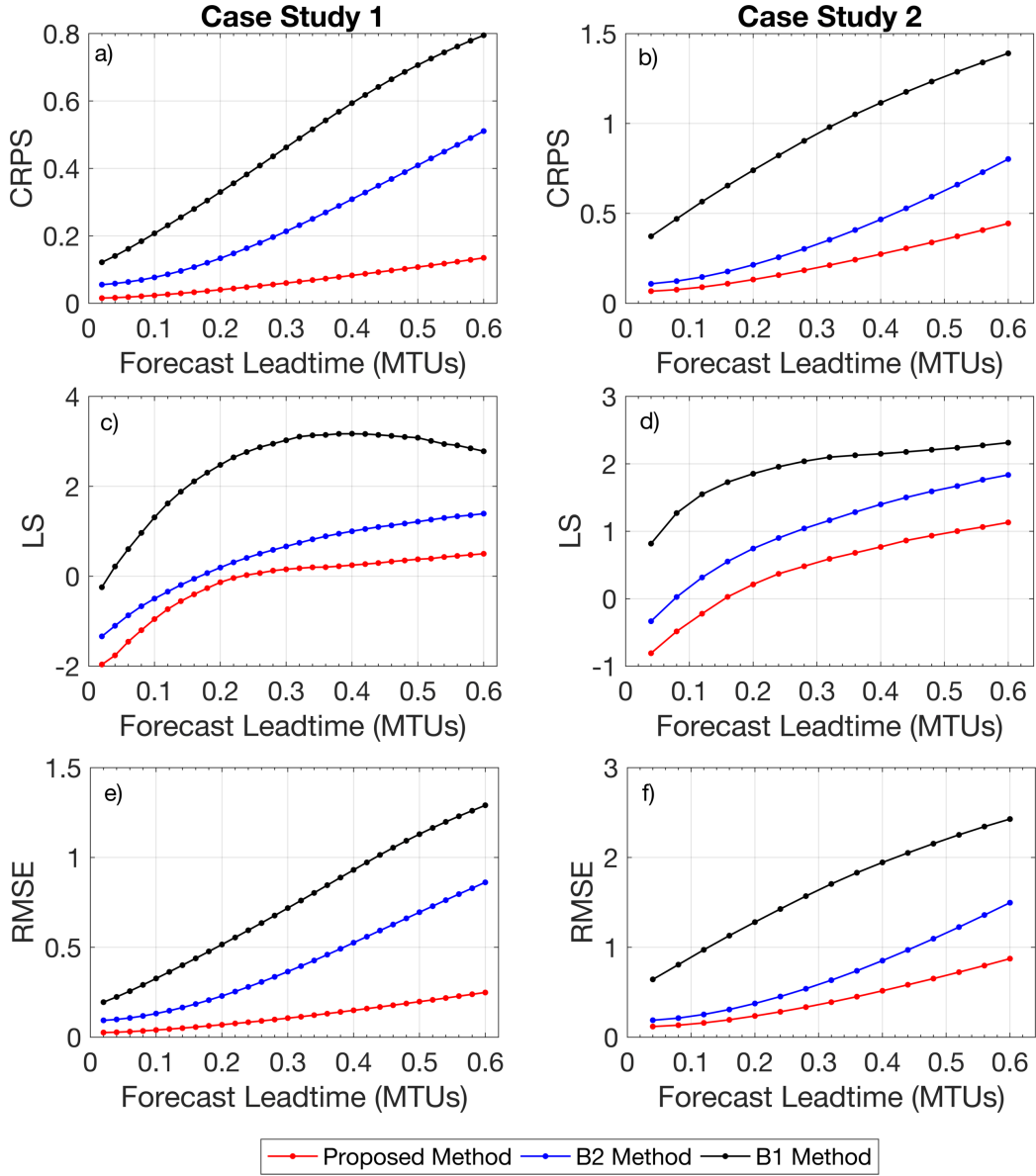


Figure 9: Forecast scores against lead time for both case studies. Scores are presented as averages across space (i.e. over all k variables) and across all simulations. Lower values indicate better performance.

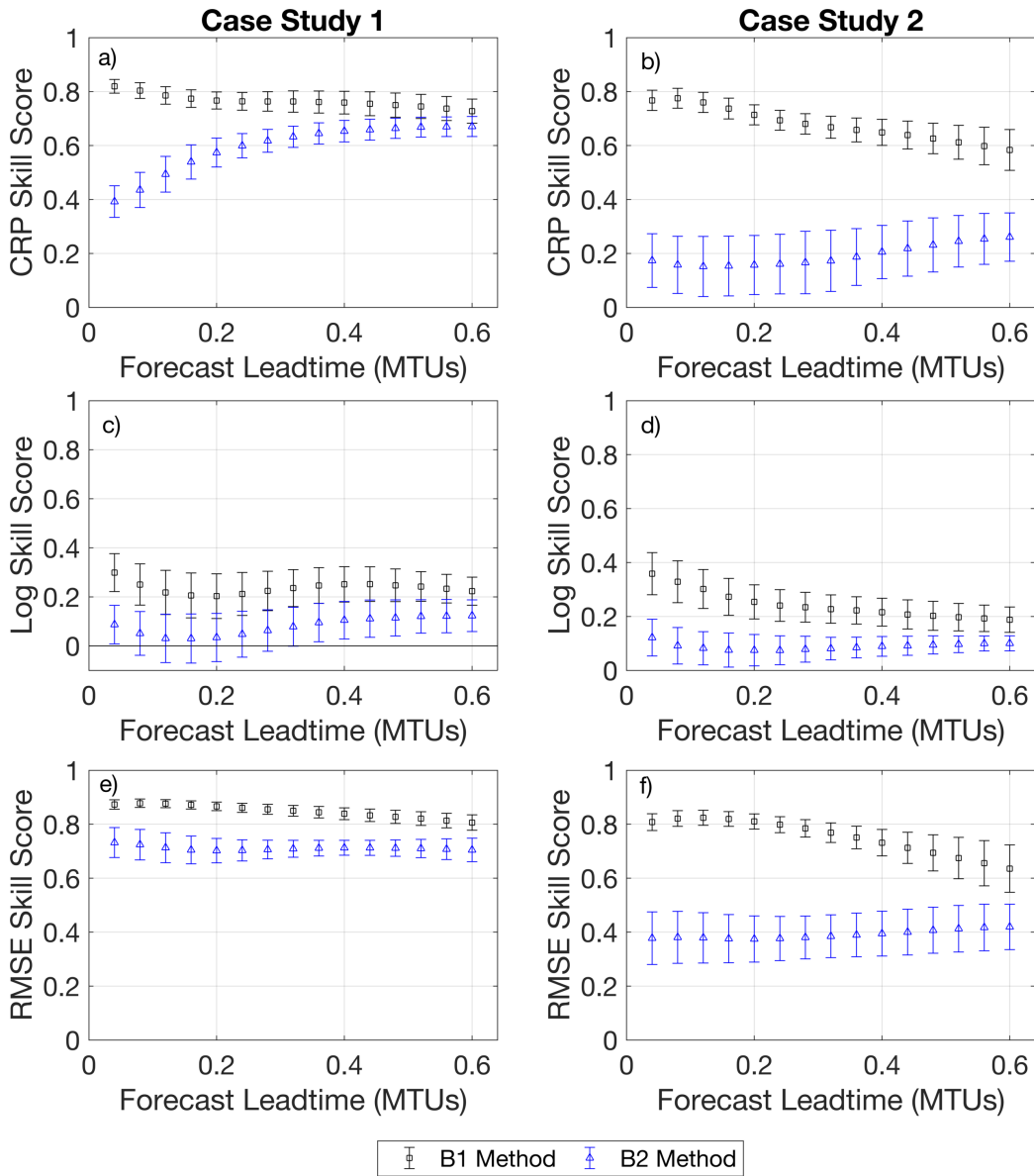


Figure 10: Forecast skill scores against lead time for both case studies. Skill scores are first averaged across space (i.e. over all k variables) and time within each independent simulation. The average of all such values over the 30 independent simulations is shown in the plot (square and triangle markers), as well as the standard deviation. More positive skill scores indicate greater relative improvement of the Proposed method compared to the benchmark method.

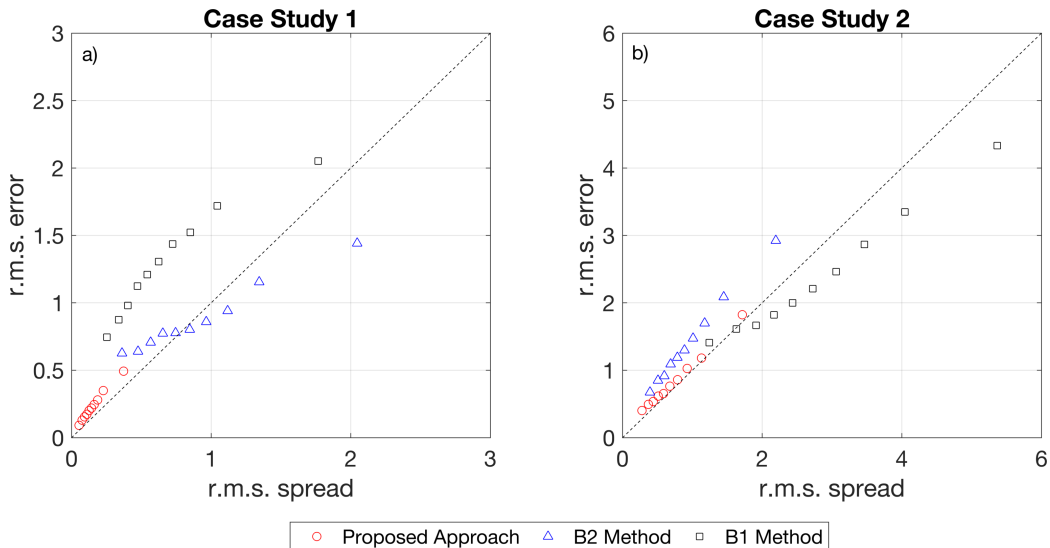


Figure 11: Forecast r.m.s error vs r.m.s spread for both case studies as a measure of statistical consistency. Results are provided for a forecast lead time of 0.6 MTU (\approx 3 days).

5. Conclusions

Characterizing model error is critical to ensure ensemble Data Assimilation methods produce high quality forecasts and analyses. Accounting for model errors due to unresolved scales is particularly of interest in weather and climate modelling. Numerous stochastic parameterization methods have been proposed for this purpose, although such methods generally rely on data or knowledge of the sub-grid scale processes and/or require observations of all resolved variables. We develop a method that is suited to the more realistic condition where the resolved variables are only partially observed and knowledge of the sub-grid processes is unavailable. It allows for the estimation of complex state dependent error structures; requires no assumptions or specification of a parametric error distribution (e.g. Gaussian errors); con-

siders the full range of statistical moments (not just bias and covariance); and avoids the need for numerical tuning typical of inflation and localization methods. The efficacy of the method is demonstrated through numerical experiments on the multi-scale Lorenz 96 model. Comparisons are made to two existing methods that use data assimilation to estimate model errors offline, as these are amenable to the partially observed setting: 1) where the errors are assumed to be Gaussian with mean and covariance estimated from a sample of analysis increments; and 2) where model errors are estimated using long window weak constraint 4D-VAR. The proposed approach is shown to recover model errors more precisely than the benchmark methods, thereby making it a more effective parameterization of the sub-grid processes. It is also particularly useful for cases with highly non-Gaussian errors, as considered in this study. Assimilation experiments with the ETKF show that the proposed approach leads to improved forecasts in terms of accuracy, reliability, resolution and consistency. The conditional variance minimization procedure in the proposed method also allows complex error structures to be estimated more precisely than with the least squares type 4D-VAR approach. The advantages of accounting for complex state dependent error relationships are also clearly demonstrated by the considerably poorer performance of the constant mean and covariance Gaussian error method.

The proposed method is suited to multi-scale systems where a locality and symmetry assumption can be made, i.e. where errors are influenced by neighbouring states instead of the full state vector and the error statistics are the same at each location in space or in parts of the state space with

similar dynamics. These assumptions help regularize the ill-posed problem of estimating model errors from partial observations. Future work will investigate systems where such assumptions are inapplicable, although it is expected that other simplifying assumptions would be needed. Finally, the method was applied to a case with negligible observation error. Subsequent work will consider the more complex case of estimating model errors from noisy observations with similar a priori assumptions considered here.

Acknowledgements

The research of S.Pathiraja has been partially funded by Deutsche Forschungsgemeinschaft (DFG) through grant CRC 1294 "Data Assimilation" and by the UNSW Faculty of Engineering Postdoctoral Writing Fellowship. PJvL acknowledges support from the EU-funded ERC grant CUNDA, and from the UK Natural Environment Research Council via National Centre of Earth Observation. We gratefully acknowledge Professor G. Gottwald and Professor S. Reich for insightful discussions during the development of this work.

References

- J. Anderson, S. Anderson, A Monte Carlo Implementation of the Nonlinear Filtering Problem to Produce Ensemble Assimilations and Forecasts, *Monthly Weather Review* 127 (1999) 2741–2758.
- T. Hamill, J. Whitaker, C. Snyder, Distance-Dependent Filtering of Background Error Covariance Estimates in an Ensemble Kalman Filter, *Monthly Weather Review* (2001) 2776–2790.

- P. Houtekamer, H. Mitchell, A Sequential Ensemble Kalman Filter for Atmospheric Data Assimilation, *American Meteorological Society* 129 (2001) 123–137.
- J. L. Anderson, An Ensemble Adjustment Kalman Filter for Data Assimilation, *Monthly Weather Review* 129 (2001) 2884–2904.
- J. L. Anderson, An adaptive covariance inflation error correction algorithm for ensemble filters, *Tellus A* 59 (2007) 210–224.
- T. Miyoshi, The Gaussian Approach to Adaptive Covariance Inflation and Its Implementation with the Local Ensemble Transform Kalman Filter, *Monthly Weather Review* 139 (2011) 1519–1535.
- X. Liang, X. Zheng, S. Zhang, G. Wu, Y. Dai, Y. Li, Maximum likelihood estimation of inflation factors on error covariance matrices for ensemble Kalman filter assimilation, *Quarterly Journal of the Royal Meteorological Society* 138 (2012) 263–273.
- S. Saha, Response of the NMC MRF model to systematic-error correction within integration, 1992.
- D. P. Dee, Online Estimation of Error Covariance Parameters for Atmospheric Data Assimilation, *Monthly Weather Review* 123 (1995) 1128–1145.
- T. Hamill, J. Whitaker, Accounting for the Error due to Unresolved Scales in Ensemble Data Assimilation :, *Monthly Weather Review* 133 (2005) 3132–3147.

- D. Dee, A. Da Silva, Data Assimilation in the presence of forecast bias, *Quarterly Journal of the Royal Meteorological Society* 124 (1998) 269–295.
- M. Lang, P. Van Leeuwen, P. Browne, A systematic method of parameterisation estimation using data assimilation, *Tellus, Series A: Dynamic Meteorology and Oceanography* 68 (2016).
- D. Zupanski, A General Weak Constraint Applicable to Operational 4DVAR Data Assimilation Systems, *Monthly Weather Review* 125 (1997) 2274–2292.
- Y. Tremolet, Accounting for an imperfect model in 4D-Var, *Quarterly Journal of the Royal Meteorological Society* 132 (2006) 2483–2504.
- M. Fisher, M. Leutbecher, G. a. Kelly, On the equivalence between Kalman smoothing and weak-constraint four-dimensional variational data assimilation, *Quarterly Journal of the Royal Meteorological Society* 131 (2005) 3235–3246.
- M. Fisher, Y. Trémolet, H. Auvinen, D. Tan, P. Poli, Weak-constraint and long window 4DVAR, *Technical Memorandum* (2011) 47.
- M. Rodwell, T. Palmer, Using numerical weather prediction to assess climate models, *Quarterly Journal of the Royal Meteorological Society* 133 (2007) 937–948.
- L. Mitchell, A. Carrassi, Accounting for model error due to unresolved scales within ensemble Kalman filtering, *Quarterly Journal of the Royal Meteorological Society* 141 (2015) 1417–1428.

- L. Mitchell, G. a. Gottwald, Data Assimilation in Slow?Fast Systems Using Homogenized Climate Models, *Journal of the Atmospheric Sciences* 69 (2012) 1359–1377.
- T. Berry, J. Harlim, Linear theory for filtering nonlinear multiscale systems with model error., *Proceedings. Mathematical, physical, and engineering sciences / the Royal Society* 470 (2014) 20140168.
- F. Lu, X. Tu, A. J. Chorin, F. Lu, X. Tu, A. J. Chorin, Accounting for model error from unresolved scales in ensemble Kalman filters by stochastic parametrization, *Monthly Weather Review* (2017) MWR–D–16–0478.1.
- R. Buizza, M. Miller, T. N. Palmer, M. Milleer, Stochastic representation of model uncertainties in the ECMWF ensemble prediction system, *Quarterly Journal of the Royal ...* 125 (1999) 2887–2908.
- T. Palmer, A nonlinear dynamical perspective on model error: A proposal for non-local stochastic-dynamic parameterization in weather and climatic prediction models, *Quarterly Journal of the Royal Meteorological Society* 127 (2001).
- G. A. Pavliotis, A. M. Stuart, *Multiscale methods: averaging and homogenization*, 2008.
- J. Wouters, S. Dolaptchiev, V. Lucarini, U. Achatz, Parameterization of stochastic multiscale triads, *Nonlinear Processes in Geophysics* 23 (2016) 435–445.
- D. Wilks, Effects of stochastic parameterizations in the Lorenz 96 system, *Quarterly Journal of the Royal Meteorological Society* 131 (2005).

- H. Arnold, I. Moroz, T. Palmer, Stochastic parametrizations and model uncertainty in the Lorenz '96 system, *Philosophical Transactions of the Royal Society A* 371 (2013).
- D. Crommelin, E. Vanden-Eijnden, Subgrid-Scale Parameterization with Conditional Markov Chains, *Journal of the Atmospheric Sciences* 65 (2008) 2661–2675.
- F. Kwasniok, Data-based stochastic subgrid-scale parametrization: an approach using cluster-weighted modelling, *Philosophical Transactions of the Royal Society A: Mathematical, Physical and Engineering Sciences* 370 (2012) 1061–1086.
- C. H. Bishop, B. J. Etherton, S. J. Majumdar, Adaptive Sampling with the Ensemble Transform Kalman Filter. Part I: Theoretical Aspects, *Monthly Weather Review* 129 (2001) 420–436.
- X. Wang, C. H. Bishop, S. J. Julier, Which Is Better, an Ensemble of Positive-Negative Pairs or a Centered Spherical Simplex Ensemble, *Bulletin of the American Meteorological Society* (2004) 2823–2829.
- G. Evensen, Sequential data assimilation with a nonlinear quasi-geostrophic model using Monte Carlo methods to forecast error statistics, *Journal of Geophysical Research* 99 (1994).
- M. K. Tippett, J. L. Anderson, C. H. Bishop, T. M. Hamill, J. S. Whitaker, Ensemble Square Root Filters*, *Monthly Weather Review* 131 (2003) 1485–1490.

- D. Marquardt, An Algorithm for Least-Squares Estimation of Nonlinear Parameters, *Journal of the Society of Industrial and Applied Mathematics* 11 (1963) 431–441.
- R. J. Hyndman, D. M. Bashtannyk, G. K. Grunwald, Estimating and Visualizing Conditional Densities, *Journal of Computational and Graphical Statistics* 5 (1996) 315–336.
- P. Hall, J. Racine, Q. Li, Cross-Validation and the Estimation of Conditional Probability Densities, *Journal of the American Statistical Association* 99 (2004) 1015–1026.
- T. Hayfield, J. Racine, Nonparametric Econometrics : The np Package, *Journal of Statistical Software* 27 (2008).
- C. E. Leith, Predictability of climate, *Nature* 276 (1978) 352–355.
- H. Li, E. Kalnay, T. Miyoshi, C. M. Danforth, Accounting for Model Errors in Ensemble Data Assimilation, *Monthly Weather Review* 137 (2009) 3407–3419.
- I. Fatkullin, E. Vanden-Eijnden, A computational strategy for multiscale systems with applications to Lorenz 96 model, *Journal of Computational Physics* 4121 (2004).
- E. Lorenz, Predictability - a problem partly solved, in: T. Palmer, R. Hagedorn (Eds.), *Predictability of Weather and Climate*, Cambridge University Press, 2006.

L. a. Smith, E. B. Suckling, E. L. Thompson, T. Maynard, H. Du, Towards improving the framework for probabilistic forecast evaluation, *Climatic Change* 132 (2015) 31–45.